https://doi.org/10.15407/ufm.22.03.382

O.K. SHUAIBOV* and A.O. MALININA**
State Institution of Higher Education 'Uzhhorod National University',
3 Narodna Sq., UA-88000 Uzhhorod, Ukraine
* alexsander.shuaibov@uzhnu.edu.ua, ** antonina.malinina@uzhnu.edu.ua

OVERSTRESSED NANOSECOND DISCHARGE IN THE GASES AT ATMOSPHERIC PRESSURE AND ITS APPLICATION FOR THE SYNTHESIS OF NANOSTRUCTURES BASED ON TRANSITION METALS

The review article presents the characteristics and parameters of an overstressed nanosecond discharge (OND) in air and argon at atmospheric pressure between electrodes made of zinc, copper, and aluminium. The technique, methods and experimental conditions for studying the characteristics and parameters of the OND and its application for the synthesis of thin nanostructured films of transition-metal oxides synthesized under intense ultraviolet (UV) irradiation of the substrate with film are presented. The microexplosions of inhomogeneities on the surface of electrodes in a strong electric field act as a source of metal vapour in plasma. The spatial, electrical, and optical characteristics of the OND in air and argon between transition-metal electrodes, which was ignited in the needle-to-needle electrode system, are reported. The results of experimental measurements of the parameters of the discharge plasma based on the Cu–air gas–vapour mixtures are presented. The optical characteristics of thin nanostructured transition-metal oxide films synthesized under conditions of automatic UV irradiation of the substrate by the discharge plasma are considered.

Keywords: overstressed nanosecond discharge, zinc, copper, and aluminium electrodes, thin nanostructured films.

Citation: O.K. Shuaibov and A.O. Malinina, Overstressed Nanosecond Discharge in the Gases at Atmospheric Pressure and Its Application for the Synthesis of Nanostructures Based on Transition Metals, *Progress in Physics of Metals*, **22**, No. 3: 382–439 (2021)

1. Introduction

Already in the initial studies of the optical characteristics of spark discharge plasma with duration of tens to hundreds of microseconds with varying degrees of overstress of the discharge gap of the 'needle-to-needle'- or 'needle-to-plane'-type, it was found that radiation from the interelectrode gap is determined mainly by the spectral lines of atoms and ions electrodes [1, 2]. Results of research of the physics of processes and the main characteristics of nanosecond atmospheric pressure discharges for the period 1960–1990 were summarized in the review [3]. In such studies, the spectral composition of the spark discharge radiation was determined mainly by the radiation of the products of electrode erosion [4]. Thus, in the spectrum of plasma radiation, which was created between copper or brass electrodes, the main radiation was concentrated in the spectral range of 200–230 nm. A detailed identification of the emission spectra was not carried out in Ref. [4]. In a spark discharge between stainless steel electrodes (d = 3.5 mm), the most intense spectral lines were in the spectral range of 240–275 nm. Subsequently, in our studies on the emission characteristics of an OND (overstressed nanosecond discharge) in the electrode system similar to that described in Refs. [3, 4], these groups of spectral lines were attributed to radiation on transitions of atoms and singly charged ions of copper and iron [5–7].

The vapour of electrode material of overstressed nanosecond discharges are introduced into the interelectrode space because of microexplosions of surface irregularities of metal electrodes in a strong electric field. Thus, during the formation of ectons [8], the use of copper and zinc is of particular interest for the development of point ultraviolet (UV) radiation sources, which are characterized the presence of intense spectral lines in the wavelength range of 200–230 nm [9, 10]. The introduction of electrode material into the interelectrode gap can also be used to synthesize thin nanostructured films of transition metals or their oxides on a dielectric substrate installed near the electrode system [11]. Especially promising can be the synthesis of nanostructured thin films of transition-metal oxides (ZnO, CuO, *etc.*) from the material of the corresponding electrodes during a discharge in air or in another oxygen-containing medium, since here automatic UV illumination of the film is realized in the process of its synthesis, which made it possible improve its electrical characteristics [12,13].

A study of the characteristics of an OND in air at atmospheric pressure between copper electrodes showed that it is a point source of UV radiation in the spectral range of 200–230 nm [7, 8]. A more detailed study of this discharge revealed that, simultaneously with UV radiation, the discharge also acted as a source of the flow of copper oxide nanostructures [14]. Nanostructures based on zinc and copper oxides

are characterized by a pronounced antimicrobial effect [15]; therefore, in the development of new methods for the simultaneous production of bactericidal UV radiation and fluxes of transition-metal nanoparticles, which enhance the inactivation and antimicrobial properties of gas-discharge air plasma, are of considerable interest for applications in microbiology, medicine and agricultural technologies. On this basis, the development of new methods for the simultaneous production of bactericidal UV radiation and fluxes of transition-metal nanoparticles is of considerable interest for applications in biomedical engineering, microbiology, medicine, and agricultural technologies.

'Point' UV lamps on metal vapour can have very small plasma volumes at the level of 1–5 mm^3; so, they are used to calibrate spectral instruments and various optical elements in the UV spectral range. The characteristics of these 'point' lamps have been most fully investigated upon excitation of discharge overvoltages with duration of 1–2 ns, when unique pump generators were used to ignite the discharge [16]. The characteristics of nanosecond discharges with metal electrodes and small nonuniformity in the distribution of the electric field in the discharge gap [17] are less studied. Such conditions are created when we use a system of electrodes of the 'sphere–sphere' type, where the radius of curvature of the working surface of the electrodes is commensurate with the value of the interelectrode distance [18]. The use of bipolar high-voltage pulses makes it possible to construct the discharge device more compact, and, at the same time, the electrode material is used more evenly when it is destroyed in a strong electric field due to the ectonic mechanism [19–27].

The results of studying overstressed discharges of subnanosecond duration with runaway electrons in gases, the pressure of which in most cases was less than the atmospheric discharge, were summarized in Ref. [28]. The results of experimental studies of the optical characteristics of the spark channel in argon at atmospheric pressure between metal electrodes, both in and without a magnetic field, are given in Refs. [29–31]. Particularly, in Ref. [31], the results of a study of the effect of a longitudinal magnetic field on the main characteristics of a spark discharge in argon at atmospheric pressure with an admixture of aluminium vapours, which were introduced into the plasma during the formation of ectons on the surface of electrodes, are presented. As shown, the magnetic field shifts the maximum of the spectral radiation density into the UV range of the spectrum, reduces the rate of expansion of the spark channel and losses to transverse radiation, and increases the specific electric power in the spark, the conductivity and temperature of the plasma at the arc stage of the discharge. This creates the prerequisites for producing 'hot' plasma and developing new gas-discharge sources of UV and x-ray radiation on its basis.

The results of studying the conditions for the synthesis of thin films based on transition metals (Cu, Zn, Fe, Al) from the products of destruction of electrodes in an overstressed nanosecond discharge of atmospheric pressure are practically absent. Therefore, the problem of studying the conditions of synthesis and the main characteristics of such films in inert and oxygen-containing gases is urgent, but this is impossible without the use of expensive laser or high-vacuum equipment.

The article reviews and summarizes the results of the study of the characteristics and parameters of plasma overstressed nanosecond discharge in the system of 'needle–needle' electrodes made of transition metals (Cu, Fe, Zn and Al) in air and high-pressure argon, as well as the results of the practical application of this type of discharge in nanotechnology and lighting engineering. Experimental study was carried out in recent years at the Department of Quantum Electronics of Uzhhorod National University.

2. Technique of Experimental Research

At the Department of Quantum Electronics of Uzhhorod National University, the studies of overstressed nanosecond discharges in high-flow gases began in 2012. They were carried out on an experimental setup, the diagram of which is shown in Fig. 1, and the diagram of the discharge module is shown in Fig. 2.

The experimental setup included a discharge module (Fig. 2), which was powered by a repetitively pulsed high-voltage source, a system for recording optical radiation based on an MDR-2 monochromator, and a system for recording pulsed electrical and optical characteristics (current, voltage, and oscillograms on the most intense spectral lines and bands) in time based on a 6-LOR multichannel wideband oscilloscope.

The discharge module was connected with metal tubes to a vacuum system, which provided a range of working gas pressures from 1 to 200 kPa.

To ignite the discharge, bipolar high-voltage pulses with duration of 50–100 ns and amplitude of ±(20–40) kV were applied to the electrodes of the discharge cell. The voltage pulse repetition rate was chosen equal to 80–100 Hz, since, at high frequencies, the discharge module was significantly heated. Oscillograms of voltage pulses across the discharge gap and oscillograms of current pulses were recorded using a broadband capacitive voltage divider, a Rogowski coil, and a 6LOR-04 broadband oscilloscope with a time resolution of 2–3 ns.

An intense nanosecond discharge between metal electrodes was ignited in a sealed discharge chamber made of plexiglas. The interelectrode distance was 1–7 mm. The chamber with the system of electrodes

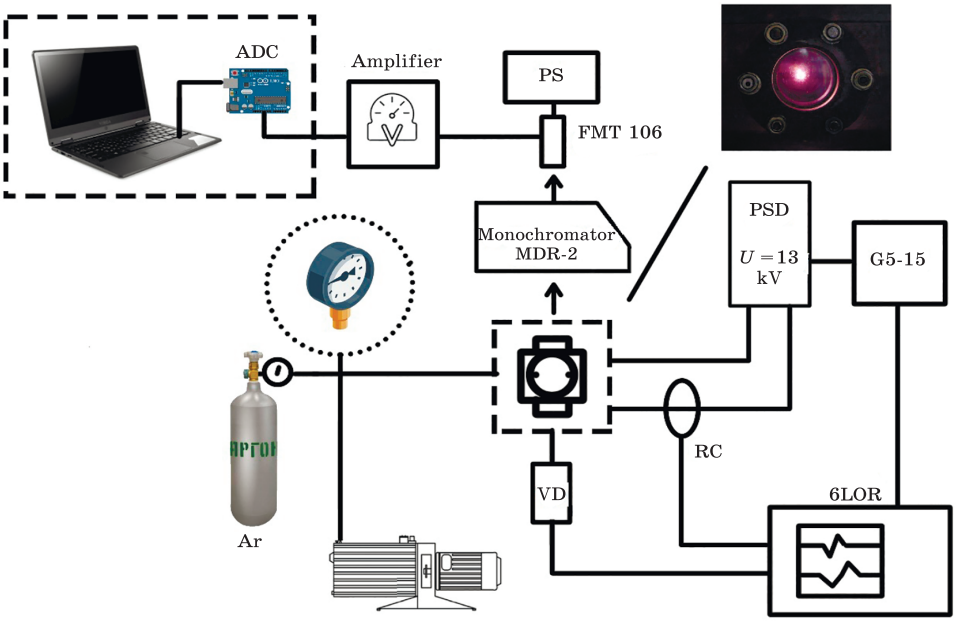

Fig. 1. Diagram of experimental setup for studying overstressed nanosecond discharge in gases: PSD is discharge power supply; FMT 106 is photoelectric multiplier tube; PS is power supply unit; ADC is analogue-to-digital signal converter; RC is Rogowski coil; VD is voltage divider to determine the voltage drop in the circuit; G5-15 is pulse generator; 6LOR is a broadband oscilloscope [32]

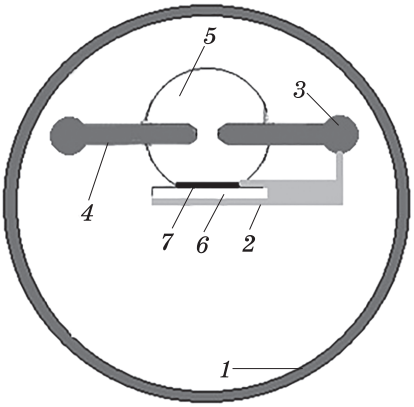

Fig. 2. Diagram of the gas-discharge module: *1* is sealed housing of the discharge chamber, *2* is substrate attachment for deposition, *3* is system for regulating the distance between electrodes, *4* is chalcopyrite electrodes, *5* is gas section where sputtering occurs, *6* is glass or quartz substrate for the deposition of thin films, *7* is a layer of the sputtered substance based on the electrode material [33]

was evacuated by a fore vacuum pump to a residual air pressure of 10 Pa, and then, air, nitrogen, or argon was filled into the chamber; the buffer gas pressure was in the range of 5–200 kPa. The diameter of the cylindrical metal electrodes is 5 mm. The radius of curvature of the working end surface of the electrodes was the same and equal to ≈3 mm. In some experiments, the discharge was ignited between electrodes made

of different metals (Cu, Zn), that made it possible to introduce vapour of different metals into the interelectrode gap.

A high-current nanosecond discharge was ignited using a bipolar high-voltage modulator of voltage pulses with a total duration of 50–150 ns and a total amplitude of positive and negative components of 40–60 kV. The voltage pulse repetition rate could vary within 40–1000 Hz, however, the main studies were carried out at a frequency of 100 Hz. Oscillograms of voltage pulses across the discharge gap and oscillograms of current pulses were recorded using a broadband capacitive voltage divider, a Rogowski coil, and a 6LOR-04 broadband oscilloscope. The time resolution of this system for measuring the characteristics of electrical pulses was 2–3 ns.

An MDR-2 monochromator and a photomultiplier (FEU-106) were used to record the emission spectra of OND plasma. The signal from the photomultiplier was fed to an amplifier and was recorded using an amplitude-digital converter in an automated system for measuring spectra on a personal computer display. The discharge radiation was investigated in the spectral range of 200–650 nm. The plasma radiation registration system was calibrated by the radiation of a deuterium lamp in the spectral range of 200–400 nm and a band lamp in the range of 400–650 nm. Oscillograms of radiation at the transitions of atoms and ions were recorded using an electronic linear multiplier ELU-14 FS, the time resolution of which was 1 ns. The pulsed electrical power of the OND was determined by graphically multiplying the oscillograms of voltage and current pulses. Time integration of the pulsed power made it possible to obtain energy in one electrical pulse, which was introduced into the plasma.

The measurement of the radiation power of the plasma of the OND was carried out using an ultraviolet meter of the absolute radiation power 'TKA-PKM', which made it possible to carry out measurements in the spectral range of 200–400 nm.

When a quartz or glass substrate was installed at a distance of 20–30 mm from the centre of the discharge gap (Fig. 2) and the discharge burning time was 1–3 hours (at f = 100 Hz), the deposition of film from the products of sputtering of the electrode material and a gas medium was recorded on the substrate. The obtained film samples were investigated for light transmission in a wide spectral region using radiation from deuterium and heat lamps (200–850 nm). These experiments were performed using a spectral complex based on an MDR-23 monochromator at room temperature according to the method descri-bed in [33].

In the system of electrodes of the 'sphere–sphere' type, at gas pressures in the range of 5–200 kPa and an interelectrode distance d = 1–3 mm, an OND in the form of a sphere was ignited, which had a diffuse form, although this discharge was initiated without using a

separate preionization system [34, 35]. For this type of discharges, a beam of 'runaway' electrons and the accompanying x-ray radiation [36, 37] can play the role of the preionization system.

The discharge was photographed using a digital camera (exposure time ≈1 s). The distance between the electrodes was used as a scale for establishing the plasma volume.

3. Characteristics of Overstressed Nanosecond Discharges

The main characteristics of overstressed discharges in high-pressure gases, which are described in the known literature, are as follow: spatial characteristics of the plasma, recorded at selected times with nanosecond accuracy or time-averaged images, voltage and current pulses, pulsed electric power of the discharge, and the energy contribution into the plasma in one discharge pulse [35].

3.1. Spatial and Electrical Characteristics

Let us consider the results of a study of the spatial and electrical characteristics of an overstressed bipolar nanosecond discharge in air and argon, which was ignited between electrodes made of copper, aluminium, and zinc.

Works [7, 34, 35] report the results of studying the spatial characteristics of an OND in the 'needle-to-needle' electrode system (at the radius of curvature of the tip commensurate with the interelectrode distance) when the discharge gap is supplied with bipolar high-voltage pulses in atmospheric pressure air between copper electrodes at different pulse repetition rates (f = 40–1000 Hz) at 1 s exposure. The mode of operation of the discharge emitter in the form of a 'point' lamp was achieved only at low repetition rates of voltage pulses (f = 40–150 Hz). With an increase in the frequency in the range of 10–150 Hz, it increased from 3 to 25 mm^3, and with a further increase in frequency to 1000 Hz, the volume of the overstressed discharge plasma grew to 100 mm^3. At pulse repetition rates in the range f = 300–1000 Hz, it was only possible a short-term operation of the discharge device, since, under these conditions, it was very hot.

The study of the spatial characteristics of an overstressed bipolar nanosecond discharge was also carried out between copper electrodes in argon at a pressure of 6.7, 100, and 150 kPa (exposure of taking images was of 1 s). At distances between the electrodes d = 2 and 7 mm, a uniform discharge with a duration of about 100–200 ns, with an amplitude of current pulses of 50–200 A and a plasma volume of 10–500 mm^3 was ignited. The discharge gap was overstressed, which created favourable conditions for formation of a high-energy runaway electron beam and accompanying x-ray radiation.

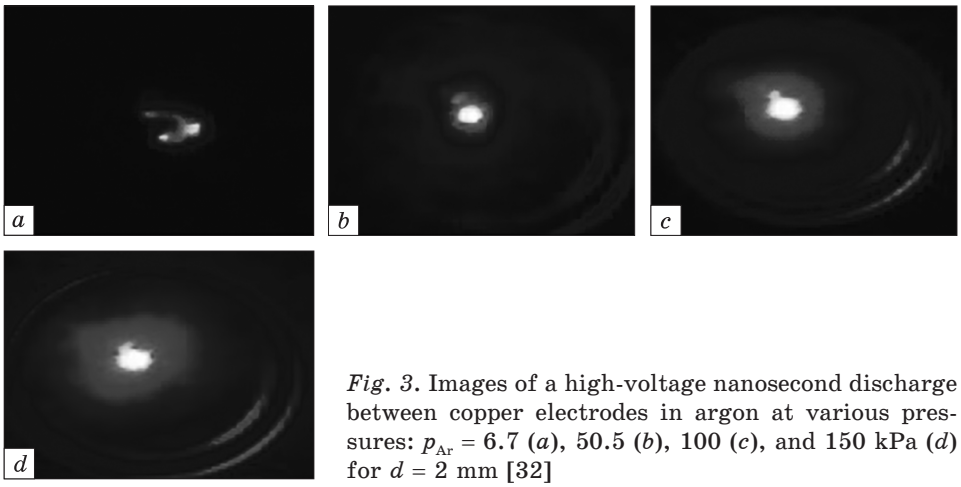

Fig. 3. Images of a high-voltage nanosecond discharge between copper electrodes in argon at various pressures: p_{Ar} = 6.7 (*a*), 50.5 (*b*), 100 (*c*), and 150 kPa (*d*) for d = 2 mm [32]

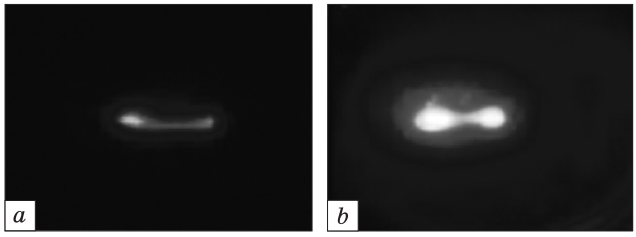

Fig. 4. Images of the OND between copper electrodes in argon at p_{Ar} = 6.7 (*a*) and 100 (*b*) kPa (d = 7 mm) [32]

Figures 3 and 4 present images of a bipolar nanosecond discharge at different argon pressures and different interelectrode distances.

At p_{Ar} = 6.7 kPa and d = 2 mm, the discharge looked like a bright central part with a diameter of about 2 mm, equal interelectrode distances and a number of weaker plasma jets moved away from the central part. With increasing the distance between the electrodes to 7 mm, the brightest part of the discharge plasma was concentrated at the tip of the needles, which were switched by a thin, less bright plasma channel. With an increase in argon pressure to 100–150 kPa, the diameter of the bright central part increased by a factor of 2–3, and the diameter of the halo that covered it increased, accordingly.

Typical oscillograms of voltage, current, and electrical pulsed power pulses of an OND between copper electrodes in argon are shown in Fig. 5. Due to the mismatch between the output resistance of the pulsed high-voltage modulator and the load (plasma) resistance, the voltage pulse had the form of individual spikes with duration of 5–10 ns. This mode of ignition of a nanosecond high-voltage discharge between metal electrodes in a 'needle-to-plane' electrode system, when the total duration of a train of 10 nanosecond voltage pulses was ≈1–1.5 μs, was used in Refs. [35–39] to generate plasma jets with material of electrodes.

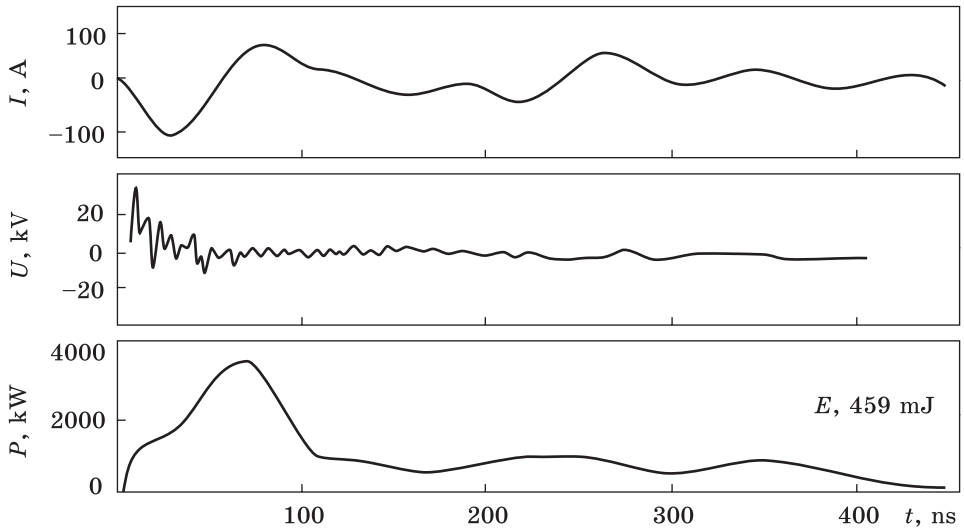

Fig. 5. Temporal (t) dependences of the pulsed electric power of the discharge (P), the voltage between the copper electrodes (U), and the current of a bipolar nanosecond discharge (I) at an interelectrode distance d = 2 mm and p_{Ar} = 150 kPa [32]

Oscillograms of voltage and current were in the form of oscillations decaying in time, which was caused by the mismatch of the output resistance of the high-voltage modulator with the load resistance. The total duration of the voltage oscillations across the gap and the discharge current reached 450 ns, with the duration of individual voltage oscillations of 7–10 ns, and the current oscillations had duration of ≈70 ns. Short-term oscillations showed up better in voltage waveforms. In the oscillograms of the current, they were partially integrated in time due to the large time constant of the Rogowski coil, which was used in these studies.

For a discharge in argon at atmospheric pressure at d = 2 mm, the amplitude of the largest voltage drop on the electrodes was achieved at the initial stage of the discharge and was ≈±7–8 kV, current — ±100 A, and pulsed power — 1.2 MW, that provided an energy contribution to one discharge pulse into the plasma circa of ≈167 mJ. With an increase in argon pressure to 150 kPa, the voltage difference of different polarity in the initial phase of the discharge at τ = 10–30 ns reached 40 kV, and the current ±80–100 A. The maximum value of the electric pulsed power reached 3.8 MW at t = 70–80 ns. The main energy contribution to the plasma was made during the first 100 ns from the moment of ignition of the discharge. The energy of one discharge pulse reached ≈470 mJ (Fig. 5).

3.2. Spectral and Temporal Characteristics

In Ref. [34], in the study of the emission characteristics of the plasma of an overstressed nanosecond discharge between zinc electrodes in air at atmospheric pressure, the broadband radiation of zinc oxide nanoparticles in the spectral range of 370–470 nm was found (for OND in a helium medium, this broadband radiation was not manifested). Therefore, it is also important to establish the possibility of manifestation of radiation of nanostructures of aluminium oxide in the UV and visible wavelengths. This will make it possible to establish the nature of continuous radiation (continuum) for atmospheric pressure plasma in gas–vapour media based on oxygen-containing gases and aluminium vapour. In an overstressed discharge of atmospheric pressure in argon-containing mixtures with aluminium or copper vapours, it is possible to synthesize nanoparticles of pure aluminium or copper in the form of these films outside the discharge plasma; therefore, it is important to know the characteristics and parameters of such plasma. The radiation of the latter can also be used as a control when comparing the discharge continuum in argon-containing and oxygen-containing gas mixtures, since aluminium-oxide nanoparticles are not formed in an inert gas environment.

The study of the spectral characteristics of the plasma radiation of a high-current nanosecond discharge in air at atmospheric pressure between electrodes made of transition metals (Zn, Cu, Al, Fe) showed that about 80–90% of its radiation power from the spectral range 200–1000 nm is concentrated in the spectral intervals 200–220 nm (electrodes with Zn), 200–230 nm (Cu), 200–260 nm (Al), 200–300 nm (Fe).

Figure 6 presents the radiation spectrum of the plasma of an overstressed bipolar nanosecond discharge between zinc electrodes in air. With a significant overvoltage of the discharge gap, when the distance between the electrodes is minimal (d = 1 mm) in air at atmospheric pressure, two groups of intense spectral lines of the zinc atom and ion in the spectral range of 200–280 nm are the main ones in the plasma radiation spectra. The most intense in the first group of spectral lines were ion lines, namely, 202.6, 206.2 nm Zn II, and in the second group, the lines of the zinc atom, namely, 250.2, 255.8 nm Zn I; this correlates well with the spectral characteristics of the lamp [40]. Compared with the data of work [40], the UV-radiation spectrum in these areas included significantly more intense spectral lines of zinc. In the near UV and visible regions of the spectrum, the spectral lines of zinc were emitted against a background of broad bands with maxima at wavelengths of 380 and 450 nm, which may be due to the emission of a zinc oxide (ZnO) molecule. These broad bands correlate well with the luminescence bands of nanostructures based on zinc oxide [40, 41].

With increasing the distance between the electrodes to d = 5 mm and atmospheric air pressure, the electric field strength in the discharge

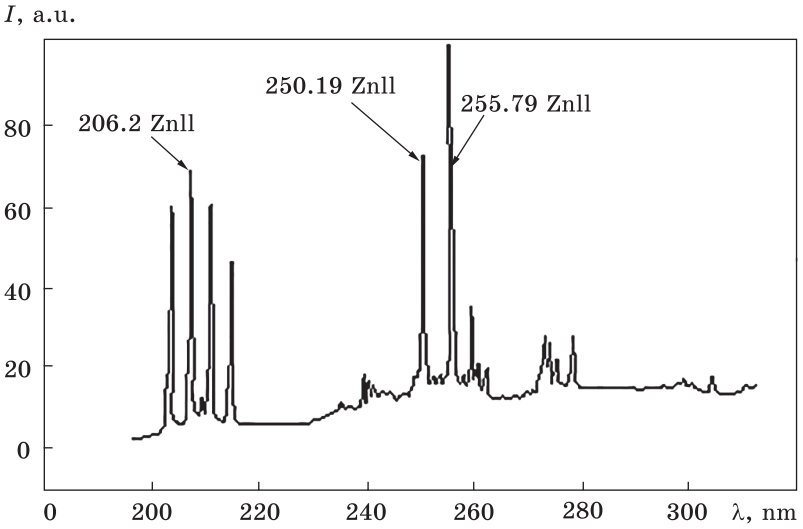

Fig. 6. Emission spectrum of plasma of the OND in air (at p = 100 kPa and d = 1 mm) [33, 34]

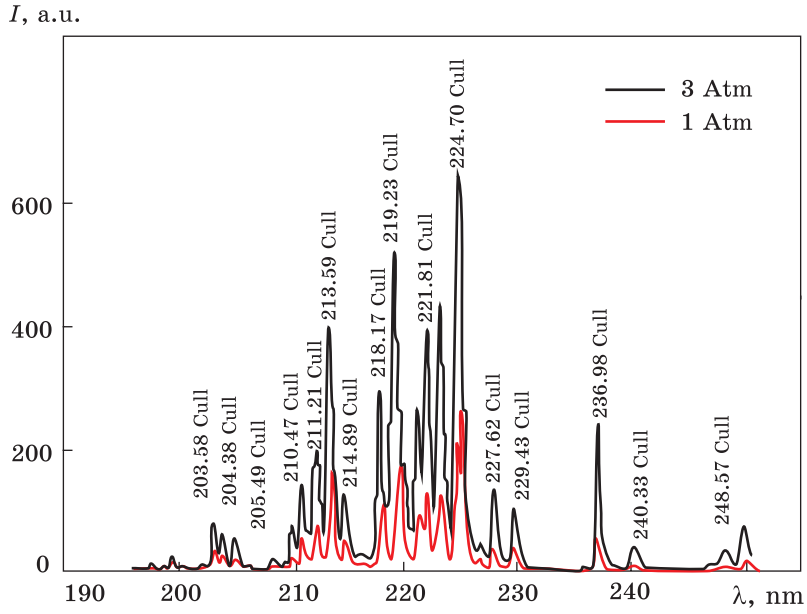

Fig. 7. Segment of the plasma emission spectrum of the OND between copper electrodes in air with the most intense spectral lines of emission of Cu atoms and ions (air pressure 10 and 300 kPa, d = 1 mm and f = 40 Hz) [33, 34]

intermediate decreases, which leads to a decrease in the electron temperature and deterioration of the conditions for x-ray preionization. In this case, the radiation intensity of the spectral lines of zinc atoms and

ions from the spectral range of 200–215 nm decreases to almost zero, and the intensity of the atomic spectral lines of zinc (from the range of 250–280 nm) decreases several times. For air plasma with small impurities of zinc vapour at d = 5 mm, the spectral lines of zinc in the wavelength ranges of 250–280 nm become the main ones (in addition to the ranges 330–350 and 460–510 nm). In the emission spectrum of the plasma of air, water vapour, and zinc, a broad band was recorded in the spectral range of 370–470 nm, which is not observed in the spectrum of plasma emission when air is replaced with helium. The maximum emission for this band is in the spectral range of 410–415 nm. This band can belong to molecules or small clusters based on zinc oxides, which are in an excited state in the gas phase.

Figure 7 presents the sections of the emission spectra (λ = 200–230 nm) of the plasma of a nanosecond discharge in air (p = 100, 30 kPa) between copper electrodes. The main emission spectra were the spectral lines of copper ions (Table 1). The UV spectrum obtained by us also correlates well with the emission range of a unipolar subnanosecond discharge [37].

Table 1. **Results of identification of the most intense spectral lines in the emission spectrum of nanosecond discharge plasma in air (p = 100 kPa) between copper electrodes (d = 1 mm). Here, λ is the wavelength, C.S.—charge state, E is the energy level, K is electronic configuration, T is term, subscripts 'u' and 'l' mean the upper and lower energy levels, I is normalized radiation intensity taking into account the spectral sensitivity of the photomultiplier and monochromator [32]**

No.	λ, nm	C.S.	E_l, eV	K_l	T_l	E_u, eV	K_u	T_u	I, a.u.
1	201.3	Cu III	9.76	$4s$	$^2D_{3/2}$	15.92	$4p$	$^2D^o_{3/2}$	56
2	202.4	Cu I	0.00	$4s$	$^2S_{1/2}$	6.12	$5p$	$^2P_{1/2}$	57
3	202.4	Cu I	0.00	$4s$	$^2S_{1/2}$	6.12	$5p$	$^2P_{3/2}$	57
4	203.5	Cu II	2.97	$4s$	$^3D_1$	9.06	$4p$	$^3D_1$	100
5	204.3	Cu II	2.71	$4s$	$^3D_3$	8.78	$4p$	$^3D_3$	52
6	205.4	Cu II	2.83	$4s$	$^3D_2$	8.86	$4p$	$^3D_2$	50
7	210.4	Cu II	2.97	$4s$	$^3D_1$	8.86	$4p$	$^3D_2$	28
8	211.2	Cu II	3.25	$4s$	$^1D_2$	9.12	$4p$	$^1P_1$	47
9	212.6	Cu II	2.83	$4s$	$^3D_2$	8.66	$4p$	$^3F_2$	55
10	213.5	Cu II	2.71	$4s$	$^3D_3$	8.52	$4p$	$^3F_4$	92
11	214.8	Cu II	8.66	$4p$	$^3F_2$	14.43	$4d$	$^3D_2$	32
12	218.1	Cu I	0.00	$4s$	$^2S_{1/2}$	5.68	$4s4p$	$^2P_{1/2}$	43
13	219.2	Cu II	2.83	$4s$	$^3D_2$	8.48	$4p$	$^3F_3$	61
14	219.9	Cu I	1.38	$4s^2$	$^2D_{5/2}$	7.02	$4p$	$^2D_{5/2}$	20
15	221.0	Cu II	3.25	$4s$	$^1D_2$	8.86	$4p$	$^3D_2$	31
16	221.8	Cu II	2.83	$4s$	$^3D_2$	8.42	$4p$	$^3P_1$	39
17	223.0	Cu I	1.38	$4s^2$	$^2D_{5/2}$	6.94	$4s4p$	$^2F_{7/2}$	31
18	224.2	Cu II	3.25	$4s$	$^1D_2$	8.78	$4p$	$^3D_3$	51
19	224.7	Cu II	2.71	$4s$	$^3D_3$	8.23	$4p$	$^3P_2$	61

In a discharge between stainless steel electrodes, the spectral lines of atoms and singly charged iron ions dominate, and the most intense is the spectral line 249.6 nm of Fe I [34]. In the emission spectrum of a discharge between copper and stainless electrodes, as well as for a discharge between two copper electrodes, the most intense emission was at the transitions of singly charged copper ions in the spectral range of 210–220 nm, and the spectral lines of iron only supplemented this spectrum in the range of 250–300 nm. The most intense in this case from the spectral lines of iron was the 271 nm line of Fe I. Such a distribution of the discharge radiation between copper and stainless steel electrodes is mainly due to different thermophysical characteristics of these metals.

The emission of spectral lines of iron was observed from the plasma of a nanosecond discharge in high-pressure helium (p = 100–500 kPa, d = 12 mm) between stainless electrodes at an overvoltage of 100–300% in the wavelength ranges 360–400 nm, 700–730 nm [42]. The shorter-wavelength range of radiation was not studied in this work. The most intense radiation of iron atoms was in the regime of a high-current diffuse discharge, when bright cathode spots were observed on the cathode surface.

To fight with various forms of the influenza virus, possibly disinfecting premises and transport with UV-radiation of lamps based on mercury atoms (mainly at a wavelength of 254 nm). They are quite effective, but they have a significant drawback, namely, they kill not only microbes and viruses, but also the cells of the human body, causing skin cancer and cataracts of the cornea of the eye. Therefore, for this application, it is possible to propose the use of a krypton chloride barrier discharge pumped gas discharge lamp, which emits at a wavelength of 222 nm, as disinfecting lamps. These lamps currently cost about $ 1000 when there is no batch production cycle. However, when installed in hospitals, public places and in transport, they are able to counteract effectively epidemics of influenza, tuberculosis and a number of others, the pathogens of which are spread by airborne droplets. The windowless UV lamp on transition metal vapour developed by us operates in normal atmospheric air and emits in the spectral range of 200–220 nm; it does not require the use of valuable gases such as krypton, corrosive gases such as chlorine, and quartz windows or sheaths. Therefore, in addition to fighting viral infections, it can be recommended for use in disaster medicine and military medicine (sterilization of medical materials and instruments, *etc.*).

Table 2 presents the results of a thorough identification of the shortest wavelength part of the spectrum (Fig. 7), which was obtained with an increased resolution of spectral lines, of a nanosecond discharge

Table 2. **Results of identification of the shortest-wavelength part of the spectrum of overstressed bipolar discharge between copper electrodes in air at atmospheric pressure. Here, λ is the wavelength, E_u is the energy of the upper level, J_u is principal quantum number, K_u is configuration, I is the radiation intensity (in relative units) taking into account the voltage sensitivity of the photomultiplier; the subscript means the pressure (in atm) [32]**

λ, nm	Object	E_u, eV	J_u	K_u	Term	I_2	I_1	$I_{0.7}$	$I_{0.3}$
197.9	Cu II	9.09	2	4*p*	3D°	—	4.5	—	—
198.9	Cu II	9.06	1	4*p*	3D°	—	4.3	—	—
199.9	Cu II	14.62	1	4*d*	3D	11.5	9.6	15.7	8.5
201.3	Cu III	15.92	1.5	4*p*	2D°	0.7	5.1	4.3	3.1
202.4	Cu I	6.12	0.5	5*p*	2P	6.7	9.6	10.7	4.9
203.5	Cu II	9.06	1	4*p*	3D	28.7	24.7	37.5	16.7
204.3	Cu II	8.78	3	4*p*	3D	22.8	17.9	31.5	13.1
205.4	Cu II	8.86	2	4*p*	3D	20.7	18.2	34.5	11.7
207.9	Cu I	7.34	1.5	8*p*	2P	3.4	13.1	8.2	10.3
208.7	Cu II	14.59	3	4*d*	3G	8.3	21.5	13.2	5.3
209.5	Cu I	7.55	0.5	11*p*	2P°	7.2	25	11.2	6.7
210.4	Cu II	8.86	2	4*p*	3D	27.1	44.3	34.1	15.8
211.2	Cu II	9.12	1	4*p*	1P	48.1	70.4	64.3	25.3
212.6	Cu II	8.66	2	4*p*	3F	72.9	89.4	94.5	33.1
213.5	Cu II	8.52	4	4*p*	3F	105.7	105.1	106.9	79.5
214.8	Cu II	14.43	2	4*d*	3D	47.6	45.2	72.2	36.3
216.5	Cu I	5.72	1.5	4*s*4*p*	2D	12	19.1	17.6	9
217.8	Cu I	5.68	1.5	4*s*4*p*	2P	20.7	77.2	100	11.7
218.1	Cu I	5.68	0.5	4*s*4*p*	2P	100.9	59.1	65.3	65.8
219.2	Cu II	8.48	3	4*p*	3F	148.8	113.1	160	92.7
219.9	Cu I	7.02	2.5	4*p*	2D	48.1	65	71.2	28.5
221.0	Cu II	8.86	2	4*p*	3D	117.6	84.9	101.8	59.5
221.8	Cu II	8.42	1	4*p*	3P	127.3	117.5	134.2	65.8
223.0	Cu I	6.94	3.5	4*s*4*p*	2F	134.8	101.8	128.7	44.4
224.2	Cu II	8.78	3	4*p*	3D	112.2	109.8	153.5	78.6
224.7	Cu II	8.23	2	4*p*	3P	152.1	128.9	169.4	100.8
226.3	Cu II	14.39	3	4*d*	3D	37.3	28.6	34	11.2
227.6	Cu II	8.42	1	4*p*	3P	77.2	45.2	76.7	19
229.4	Cu II	8.23	2	4*p*	3P	87.4	47.8	68.2	29.4
231.9	Cu I	6.98	1.5	4*s*4*p*	2P°	11.5	13.8	13.2	9.4
233.6	Cu II	14.43	2	4*d*	3D	12	12.5	11.2	7.1
235.5	Cu II	13.68	2	5*s*	1D	15.8	14.6	14.7	8.5
236.9	Cu II	8.48	3	4*p*	3F	88.5	59.4	99.5	31.7
240.3	Cu II	13.39	3	5*s*	3D	29.8	26.8	31	13.1
242.4	Cu II	13.64	1	5*s*	3D	13.1	16.7	16.7	9
244.1	Cu I	5.07	0.5	4*s*4*p*	4P°	13.1	18.5	16.5	10.3
246.8	Cu III	24.06	3.5	5*s*	4F	14.7	21.1	19.1	9.4
247.3	Cu II	13.43	2	5*s*	3D	23.9	25.3	22.1	11.7
248.5	Cu II	13.64	1	5*s*	3D	33	31.8	31.1	13.1

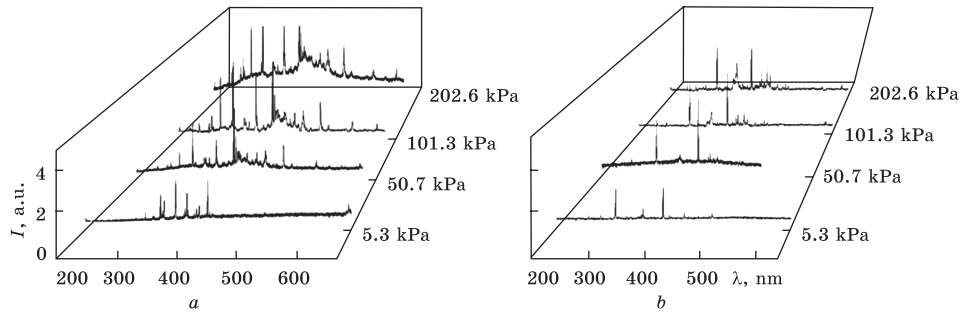

Fig. 8. Plasma emission spectra of the OND between aluminium electrodes at various pressures of air (*a*) and argon (*b*): 5.3, 50, 100, and 200 kPa [42–44]

Table 3. **Result of deciphering the emission spectrum of the discharge between aluminium electrodes in argon at atmospheric pressure (Fig. 9, *b*) [32]**

Wavelength λ, nm	Particle	Transition	Terms	Lower energy level, eV	Upper energy level, eV
308.21	Al I	$3s_2(^1S)3p–3s_2(^1S)3d$	$2P^*–2D$	0.000000	4.021485
309.27	Al I	$3s_2(^1S)3p–3s_2(^1S)3d$	$2P^*–2D$	0.013893	4.021651
309.28	Al I	$3s_2(^1S)3p–3s_2(^1S)3d$	$2P^*–2D$	0.013893	4.021485
394.40	Al I	$3s_2(^1S)3p–3s_2(^1S)4s$	$2P^*–2S$	0.000000	3.142722
394.89	Ar I	$3s^23p^5(2P^*\langle 3/2\rangle)4s–3s^23p^5(2P^*\langle 3/2\rangle)5p$	$2[3/2]^*–2[1/2]$	11.548350	14.687120
396.15	Al I	$3s_2(^1S)3p–3s_2(^1S)4s$	$2P^*–2S$	0.013893	3.142722
415.85	Ar I	$3s^23p^5(2P^*\langle 3/2\rangle)4s–3s^23p^5(2P^*\langle 3/2\rangle)5p$	$2[3/2]^*–2[3/2]$	11.548350	14.528910
419.83	Ar I	$3s^23p^5(2P^*\langle 3/2\rangle)4s–3s^23p^5(2P^*\langle 3/2\rangle)5p$	$2[3/2]^*–2[1/2]$	11.623590	14.575950
420.06	Ar I	$3s^23p^5(2P^*\langle 3/2\rangle)4s–3s^23p^5(2P^*\langle 3/2\rangle)5p$	$2[3/2]^*–2[5/2]$	11.548350	14.499050

between copper electrodes in air at various air pressures in the discharge gap. As follows from the data in Table 2, the intensity of the spectral lines of atoms and ions reached a maximum at an air pressure of 70 kPa.

Figure 8, *a*, *b* presents the emission spectra of plasma of an overstressed nanosecond discharge between aluminium electrodes in air and argon [42, 43]. Experiments with argon, which were carried out in the same current range as with air, were carried out in order to demonstrate the absence of emission bands of nanostructures of aluminium oxides in the plasma of inert gases (where there are no oxygen carriers). The spectra are shown in Fig. 8, *a*, *b*, recorded under the same conditions of discharge excitation and under the same conditions of registration. Therefore, the intensities of the same spectral lines and bands in different spectra can be compared with each other in magnitude. The results

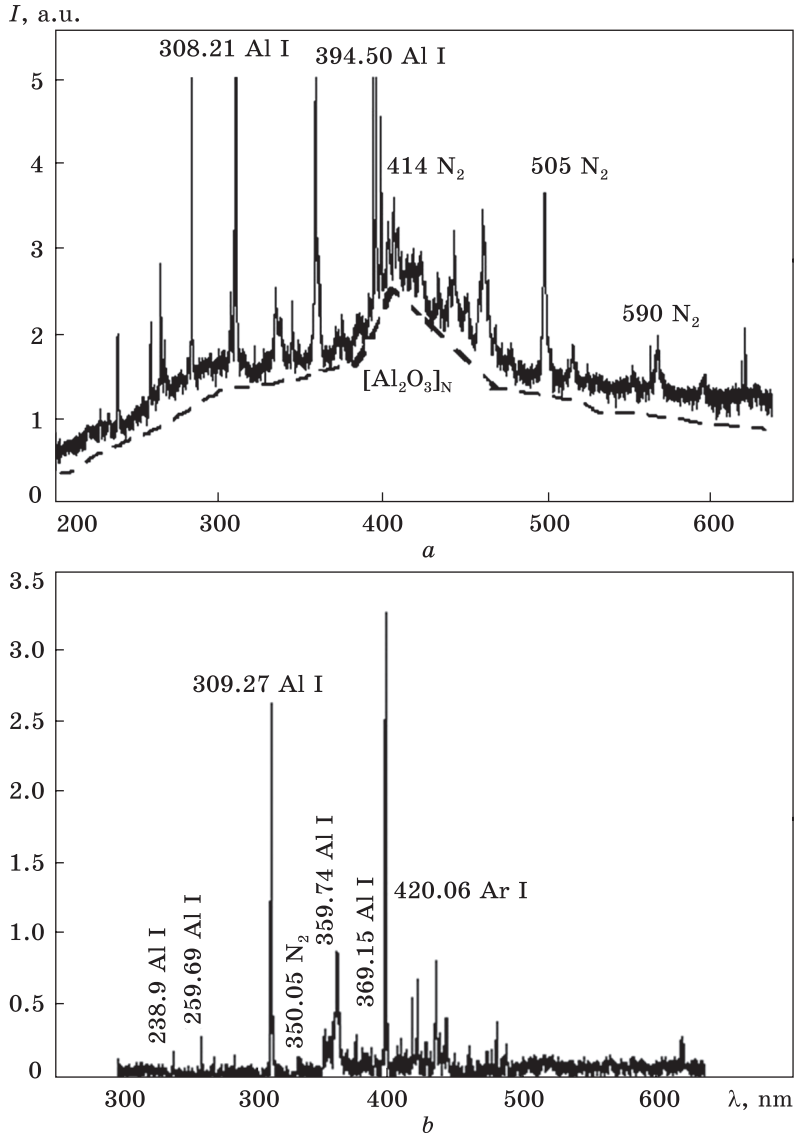

Fig. 9. Plasma emission spectra of the OND between aluminium electrodes at air (*1*) and argon (*2*); the pressures equals to 100 kPa; dashed line designates aluminium oxide nanoparticles [43, 44]

of the identification of the spectral lines of aluminium, which were emitted by plasma based on a mixture of argon with an admixture of aluminium vapour, are given in Table 3.

As follows from Fig. 8, the emission intensity of the discharge plasma in air at all pressures under investigation was dominated by the

emission intensity of the spectral lines and bands of the discharge in argon. In the emission spectra of air plasma with a small admixture of aluminium vapours, radiation was recorded at the transitions of an atom and a singly charged aluminium ion, radicals of nitrogen oxides and nitrogen molecules, as well as in the plasma emission spectra of an overstressed unipolar nanosecond discharge between aluminium electrodes in nitrogen [38]. In the argon-based discharge, mainly radiation was recorded at the transitions of the atom and the aluminium ion (Fig. 8, *b*).

The most intense spectral lines of the atom and singly charged ion of aluminium, which appeared in the spectra of plasma radiation, were as follow: (256.8 + 257.5 + 257.5) 265.3, 394.4, 396.2 nm Al I; 236.5, (247.5 + 247.6) 286.9, 622.6, (623.1 + 624.3) nm Al II.

Figure 9 presents the emission spectra of the plasma of an OND between aluminium electrodes in the air–aluminium vapour gas–vapour mixture. Experiments with argon, which were carried out at the same pressure as with air (p = 100 kPa), allowed to demonstrate the absence of emission bands of nanostructures of aluminium oxide in argon plasma. It follows from Fig. 9 that, in the emission spectra of plasma based on air with a small admixture of aluminium vapour, emission was observed at the transitions of the atom and singly charged ion of aluminium, nitrogen oxide and nitrogen molecules.

In the emission spectra of the plasma of an OND in air mixtures with a small admixture of aluminium vapours (Fig. 9, *a*), broad emission bands were recorded with maxima in the spectral ranges of 410–420 nm and 300–390 nm. The maximum radiation intensity of these bands was obtained at an air pressure of 200 kPa. In a discharge in mixtures with argon, these bands were absent in the emission spectra of the discharge.

In Ref. [45], typical electroluminescence spectra of anodic aluminium oxide are presented. These spectra were in the form of broad luminescence bands in the spectral range with maxima in the spectral range of 480–550 nm. Proceeding from this, the most probable source of broadband radiation from the plasma of the discharge under investigation can only be nanostructures of aluminium oxide.

It was noted in Ref. [46] that a broad emission band with a maximum at λ = 415 nm was observed in the photoluminescence spectrum of anion-defective single crystals and nanostructured ceramics based on alumina upon excitation of the corresponding samples by radiation with λ = 205 nm. This band coincides with that obtained in this experiment. It is interpreted as the emission band of F-centres (transition $1S$–$3P$ with a maximum emission spectrum at an energy of 3.0 eV and a decay time constant of 36–40 ms) [47, 48]. In Ref. [45], the results of studying the cathodoluminescence spectra of nanostructured ceramics of alu-

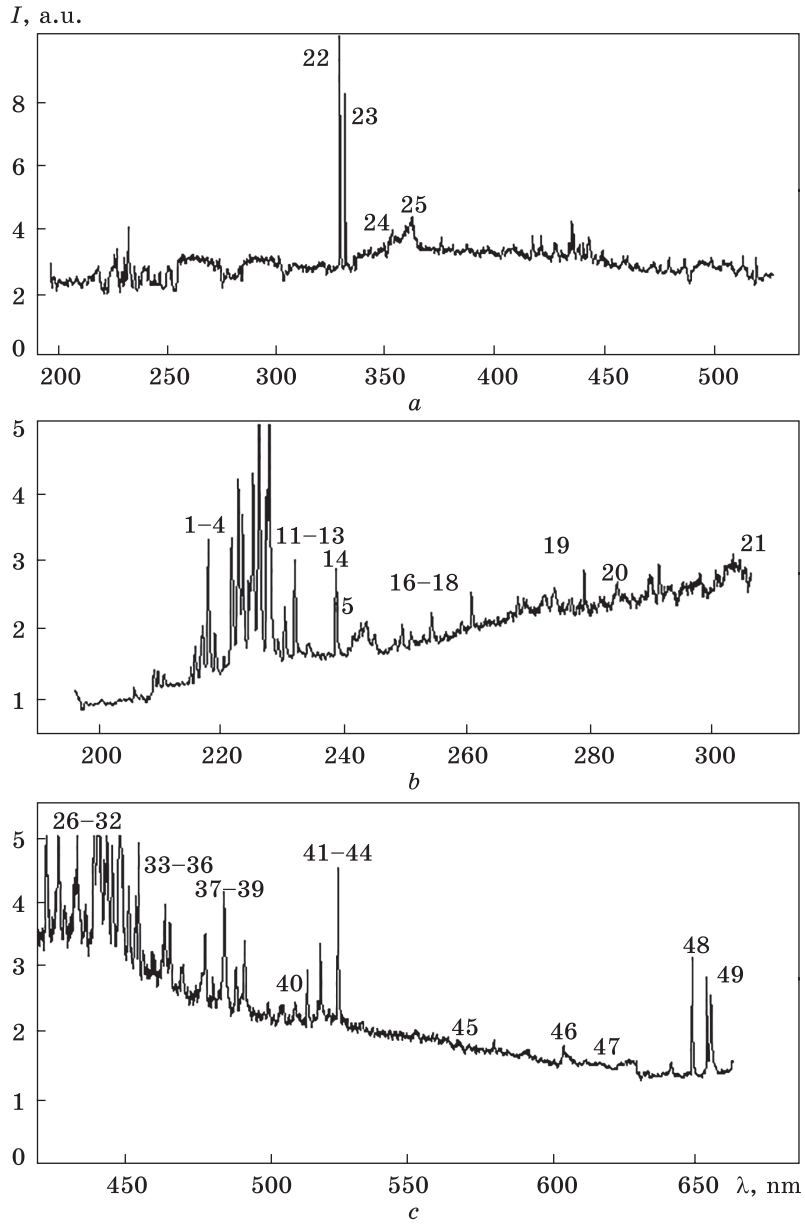

Fig. 10. The emission spectrum of a high-voltage nanosecond discharge in argon between copper electrodes at d = 2 mm and p_{Ar} = 100 kPa [32]

minium oxide are also presented. Cathodoluminescence was excited by a pulsed electron beam with a density of 1 A $\cdot$cm^{-2}, an energy of 180 keV, and a duration of 3 ns. The spectrum of this cathodoluminescence coincided with the range obtained in our experiment at air pressures of

100–200 kPa. The main one here was the band with a maximum at λ = 410–420 nm (photon energy 3.0 eV), which was adjacent to a wider short-wavelength band with maxima of the photon energy at 3.4, 3.8, 4.3 eV. The UV-photocathodoluminescence bands of nanostructured alumina ceramics are caused by the emission of F^+-centres created by oxygen vacancies and are characterized by a relatively short decay time at the level of (0.6–1.0 μs) [45, 46].

As found, the plasma of an overstressed nanosecond discharge, formed under the action of a packet of 5–10 ns voltage pulses with a duration of 100–120 ns, between aluminium electrodes at an air pressure of 50–202 kPa is characterized by a discharge pulsed power of 3–6.5 MW and an energy contribution per pulse ≈110–153 mJ. For a discharge in a mixture of nitrogen and oxygen (100–1) at pressures p = 50–101 kPa, the pulsed power of the discharge was 3–6.3 MW with an energy contribution of 110–153 mJ in the pulse. In both cases, the plasma was the source of luminescence of nanoparticles of aluminium oxide in the form of a broad band, which is in the spectral range of 300–430 nm. Broad luminescence bands from the plasma of the investigated discharge were found, assigned to the radiation of the F^-- and F^+-centres of oxygen vacancies of nanostructured aluminium-oxide ceramics.

We consider the electrical, optical, and temporal characteristics of the radiation of a discharge between copper electrodes in argon at atmospheric pressure.

The oscillograms of voltage and current had the same form as for a discharge in air between copper electrodes. For a discharge in argon at atmospheric pressure at d = 2 mm, the amplitude of the largest voltage drop on the electrodes reached at the initial stage of the discharge was ≈±7–8 kV, for current, ±100 A, and for pulsed power, 1.2 MW that provided an energy contribution to one discharge pulse into the plasma of ≈167 mJ.

Figure 10 presents the emission spectrum of a high-voltage nanosecond discharge between copper electrodes, which was ignited at p_{Ar} = 100 kPa and a distance between the electrodes of 2 mm. The results of spectrum identification (Fig. 10) are summarized in Table 4.

A feature of these emission spectra was the presence of a continuum, against which all spectral lines and bands were observed. The continuum was most pronounced at atmospheric pressure of argon (Fig. 10). The nature of this continuum under the conditions of our experiment is associated with thermal and recombination plasma radiation. The shape of the continuum with a wide maximum at 400–450 nm correlated well with the results known from the literature. Thus, in Ref. [20], for a spark discharge in argon at atmospheric pressure between aluminium electrodes (at d = 10 mm), an intense continuum was recorded in the

Table 4. **Results of deciphering the plasma emission spectra of a high-voltage nanosecond discharge between copper electrodes at p_{Ar} = 100 kPa and d = 2 mm [32]**

No.	λ_{tabl}, nm	I_{exp}, a.u.	Object	E_{low}, eV	E_{up}, eV	Lower term	Upper term
1	214.89	1.78	Cu II	1.39	7.18	$4s^2\ ^2$D	$5f\ ^2$F°
2	216.50	2.07	Cu I	0.00	5.72	$4s\ ^2$S	$4p'\ ^2$D°
3	217.49	3.34	Cu II	8.92	14.61	$4p\ ^1$F°	$4d\ ^1$G
4	220.05	1.63	Cu II	9.06	14.70	$4p\ ^3$D°	$4d\ ^3$F
5	221.02	3.34	Cu II	3.26	8.86	$4s\ ^1$D	$4p\ ^3$D°
6	221.45	4.21	Cu I	1.39	6.98	$4s^2\ ^2$D	$4p''\ ^2$P°
7	223.84	3.69	Cu I	1.64	7.18	$4s^2\ ^2$D	$5f\ ^2$F°
8	224.70	4.30	Cu II	2.72	8.23	$4s\ ^3$D	$4p\ ^3$P°
9	226.30	5.00	Cu I	1.64	7.12	$4s^2\ ^2$D	$7p\ ^2$P°
10	227.62	5.05	Cu II	2.98	8.42	$4s\ ^3$D	$4p\ ^3$P°
11	229.43	1.89	Cu II	2.83	8.23	$4s\ ^3$D	$4p\ ^3$P°
12	230.31	2.34	Cu I	1.64	7.02	$4s^2\ ^2$D	$4p''\ ^2$D°
13	236.98	1.82	Cu II	3.26	8.49	$4s\ ^1$D	$4p\ ^3$F°
14	239.26	2.86	Cu I	1.64	6.82	$4s^2\ ^2$D	$6p\ ^2$P°
15	244.16	2.12	Cu I	0.00	5.08	$4s\ ^2$S	$4p'\ ^4$P°
16	249.21	2.08	Cu I	0.00	4.97	$4s\ ^2$S	$4p'\ ^4$P°
17	254.48	2.25	Cu II	8.52	13.39	$4p\ ^3$F°	$5s\ ^3$D
18	261.83	2.55	Cu I	1.39	6.12	$4s^2\ ^2$D	$5p\ ^2$P°
19	279.17	2.86	Cu II	14.33	18.77	$4d\ ^3$G	$6f\ ^3$H°
20	282.43	2.5	Cu I	1.39	5.78	$4s^2\ ^2$D	$4p'\ ^2$D°
21	306.34	3.13	Cu I	1.64	5.68	$4s^2\ ^2$D	$4p'\ ^2$P°
22	324.75	9.98	Cu I	0	3.82	$4s\ ^2$S	$4p\ ^2$P°
23	327.39	8.19	Cu I	0	3.39	$4s\ ^2$S	$4p\ ^2$P°
24	354.89	4.10	N_2	Second positive system $C^3\Pi_u^+$–$B^3\Pi_g^+$ (3; 2)			
25	357.69	4.37	N_2	Second positive system $C^3\Pi_u^+$–$B^3\Pi_g^+$ (0; 1)			
26	420.06	5.04	Ar I	11.55	14.50	$4s$ [S]°	$5p$ [2S]
27	425.93	4.99	Ar I	11.83	14.74	$4s'$ [S]°	$5p'$ [S]
28	430.01	3.95	Ar I	11.62	14.51	$4s$ [1S]°	$5p$ [1S]
29	433.35	5	Ar I	11.83	14.69	$4s'$ [S]°	$5p'$ [1S]
30	436.37	3.97	Ar I	11.62	14.46	$4s$ [1S]°	$5p$ [S]
31	442.39	5.13	Ar I	11.72	14.52	$4s'$ [S]°	$5p'$ [1S]
32	451.07	4.25	Ar I	11.83	14.58	$4s'$ [S]°	$5p$ [S]
33	459.60	3.25	Ar I	11.83	14.52	$4s'$ [S]°	$5p'$ [1S]
34	460.95	3.32	Ar II	18.45	21.14	$4s'\ ^2$D	$4p'\ ^2$F°
35	462.84	3.96	Ar I	11.83	14.51	$4s'$ [S]°	$5p$ [2S]
36	470.23	3.03	Ar I	11.83	14.46	$4s'$ [S]°	$5p'$ [1S]
37	483.66	4.18	Ar I	12.91	15.47	$4p$ [S]	$9s$ [1S]
38	487.62	3.01	Ar I	12.91	15.45	$4p$ [S]	$7d$ [1S]
39	492.10	3.39	Ar I	13.09	15.61	$4p$ [2S]	$10d$ [3S]
40	511.82	2.47	Ar I	13.09	15.52	$4p$ [2S]	$6d'$ [2S]°
41	516.22	2.98	Ar I	12.91	15.31	$4p$ [S]	$6d$ [S]
42	518.77	3.36	Ar I	12.91	15.30	$4p$ [S]	$5d'$ [1S]°
43	521.82	2.4	Cu I	3.82	6.19	$4p\ ^2$P°	$4d\ ^2$D
44	525.27	4.53	Ar I	13.09	15.45	$4p$ [2S]	$7d$ [3S]
45	570.02	1.96	Cu I	1.64	3.82	$4s^2\ ^2$D	$4p\ ^2$P°
46	601.36	1.92	Ar I	13.08	15.14	$4p$ [2S]	$5d$ [S]°
47	617.01	1.84	Ar I	13.17	15.18	$4p$ [1S]	$7s$ [1S]°
48	653.81	3.17	Ar I	13.08	14.95	$4p$ [2S]	$4d'$ [S]°
49	659.61	2.85	Ar I	13.08	14.95	$4p$ [2S]	$4d'$ [S]°

emission spectrum in the wavelength range of 350–460 nm with a maximum at λ = 420 nm. The continuous spectrum of plasma radiation began to be recorded after a time interval Δt = 40 ns from the beginning of the discharge, when the intensity of the argon ion lines began to increase sharply.

The maximum intensity of the continuous spectrum Ar II spectral lines was achieved after a time interval Δt = 300–400 ns from the onset of a sharp increase in the current [20, 21].

At the stage of slow expansion of the spark channel, starting from the time instant 500 ns, the intensity of the continuum decreased, as for the intensity of the ionic spectral lines of argon, and the intensity of the atomic lines: 394.9, 308.2 nm Ar I and lines of the electrode material (281.6, 289.1 nm Al II) grew [30].

In the emission spectra of the discharge plasma (Fig. 10) on a mixture of argon with copper vapour in the UV-wavelength range of 214–330 nm (lines 1–23; Table 4), the emission at the transitions of the atom and singly charged Cu ion was observed. The most intense ionic spectral line was the line with λ = 227.62 nm Cu II, and the atomic intense lines were the resonance spectral lines of the copper atom with λ = 324.75 and 327.39 nm Cu I, in which the lower energy level is the ground level. The highest energy of the upper level for the Cu II lines was $E_{up.}$ = 18.77 eV, and for atomic lines, the maximum energy of the upper level was $E_{up.}$ = 7.18 eV. In the UV spectrum, bands of the second positive system of the nitrogen molecule were also observed, since, in these experiments, the discharge chamber was evacuated only to a residual air pressure of ≈10 Pa. In the wavelength range of 360–659 nm, radiation was observed mainly at the transitions Ar I, Ar II, as well as an intense spectral line of the hydrogen atom (λ = 656.29 H_α), which is due to the residual air pressure in the chamber after it was pumped out by a foreline pump.

When the distance between the electrodes is 2 mm and a bipolar generator of high-voltage nanosecond pulses is used, one or several (with a strong overvoltage of the discharge gap) cathode spots are formed, moving one towards the other.

For a high-voltage nanosecond discharge in argon at atmospheric pressure, some optical and gas-dynamic characteristics of the cathode spot plasma were given in Refs. [29, 30]. However, in these experiments carried out at an interelectrode distance d = 10 mm between the aluminium electrodes, the radiation of the cathode spot plasma with a diameter of ≈0.2–0.3 mm and, attached to it, the diffuse discharge plasma, which occupied in the most of the discharge gap, was clearly recorded. The formation of cathode spots in an OND is explained by the explosive emission model, which is based on the introduction of significant energy at the microtips of the cathode surface with their subse-

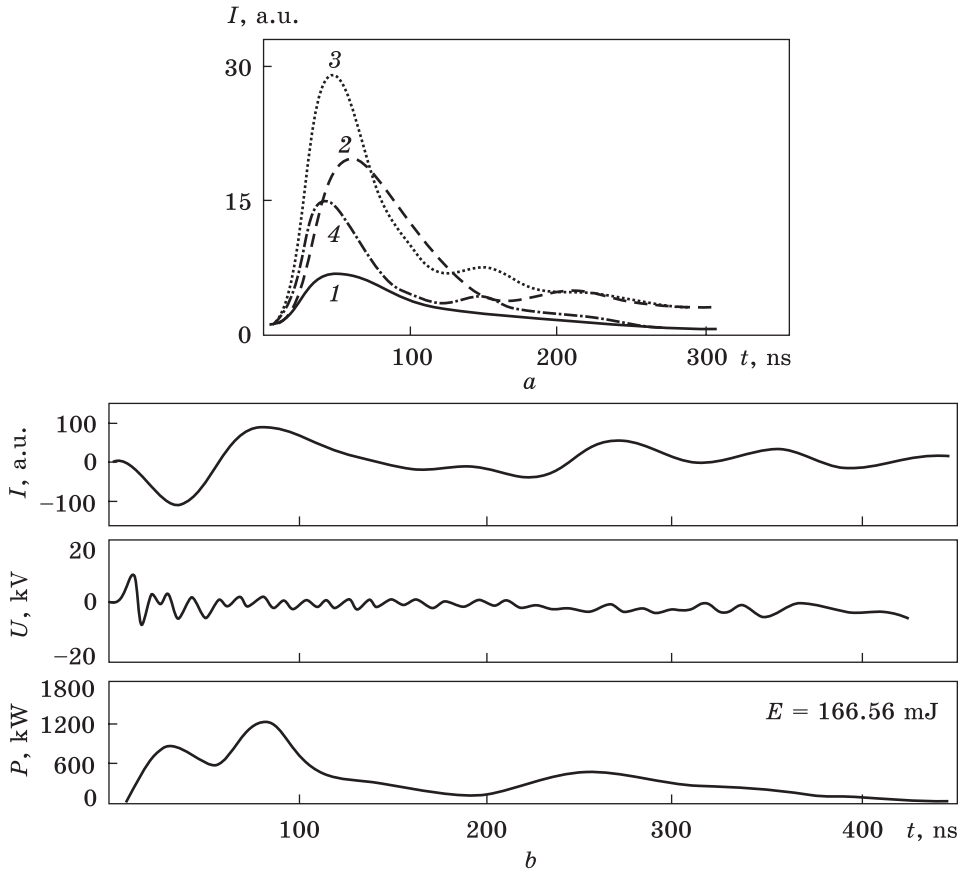

Fig. 11. Oscillograms of the luminescence at the transitions of Cu and Ar atoms (*a*): *1* — 249.1 nm Cu I, *2* — 306.34 nm Cu I, *3* — 470.23 nm Ar I, *4* — 521.82 nm Cu I; and oscillograms of current, voltage across discharge gap, and electric pulsed discharge power (*b*) at p_{Ar} = 100 kPa, d = 2 mm [32]

quent heating and explosion. The cathode spot was formed simultaneously with the onset of a sharp increase in the current and a drop in voltage across the gap, and at the initial stages of formation, it was hemispherical and had a low expansion rate of $\approx 2.5 \cdot 10^6$ cm/s. The kinetic energy of 50–100 eV corresponded to this speed of movement of the cathode spot, at which an 'ecton' with the number of electrons of 10^{11}–10^{12} and a conglomeration of metal vapour were formed. At the initial stage of the discharge, the radius of the cathode spot did not predominate $\approx 10^{-6}$ m, and, with time t from 5 to 50 ns, it increased from 0.5 to $4.3 \cdot 10^{-4}$ cm [29]. The temperature of electrons near the cathode argon plasma at atmospheric pressure, which was estimated from the relative intensity of emission of spectral lines of argon, at the initial moments of its formation (at a time interval of ≈30–40 ns) reached 5 eV

and, at subsequent moments of time (τ = 50–500 ns) decreased from 4.2 to 3.4 eV [30]. The main part of the discharge energy is introduced into the cathode spot in the plasma phase, therefore, in the plasma conglomeration, it scatters, and the energy is first introduced into the electronic component with the subsequent transfer of this energy from electrons to ions. Therefore, the mechanism of the excited Cu ions in the plasma formation can be determined *via* processes of their excitation by electrons from the ground state of the corresponding ion. The effective cross sections for the excitation of transition metal ions by electron impact are large and, for example, for zinc ions, they reach 10^{-16} cm^2 [48]. There are no data on the effective cross sections for the excitation of a copper ion in the ground energy state by electron impact in the literature known to us, which may be due to the difficulty of obtaining stable beams of copper ions suitable for measuring the corresponding effective cross sections.

The reason for these processes is the high concentration of electrons in the plasma of overstressed discharges of nanosecond duration with an ectonic mechanism of electrode sputtering, which reaches 10^{17} cm^{-3} [49]. Estimates of the concentration of electrons in a spark discharge in argon at atmospheric pressure, carried out in [30], from the experimentally determined half-width of the spectral line Ar II: $\Delta\lambda$ = 0.42 nm, showed that it is $\approx 2.4 \cdot 10^{18}$ cm^{-3}.

Figure 11 presents oscillograms of radiation at the transitions of the most intense spectral (resonance) lines of the copper atom and the bands of the second positive system of the nitrogen molecule at an argon pressure of 100 kPa.

The emission from the transitions of the copper atom was in the afterglow of the first maximum of the pulsed power, weak second luminescence maxima were recorded only for spectral lines with λ = 306.34, 521.82 nm Cu I at t = 150 ns. It is likely that, at atmospheric pressure of argon, the duration of the diffuse stage of the high-voltage nanosecond discharge prevailed 100 ns, and the second maximums of the luminescence of the lines of the copper atom appear already at the contracted stage of the discharge. Such a picture of the development of such discharges was established in Ref. [36] during high-speed photography of the discharge with nanosecond time resolution. The absence of a repeated maximum in the oscillogram of the spectral line of 249.1 nm of Cu I, of which the lower is the main energy level of the copper atom, can be due to the process of self-absorption of radiation at the channel stage of the discharge, when the concentration of copper vapour in the plasma increases. Radiation at the transition of the argon atom with λ = 470.23 nm Ar I, also observed in the afterglow of the first maximum of the pulsed power of the discharge, can be determined by the recombination mechanism of population of its upper energy level.

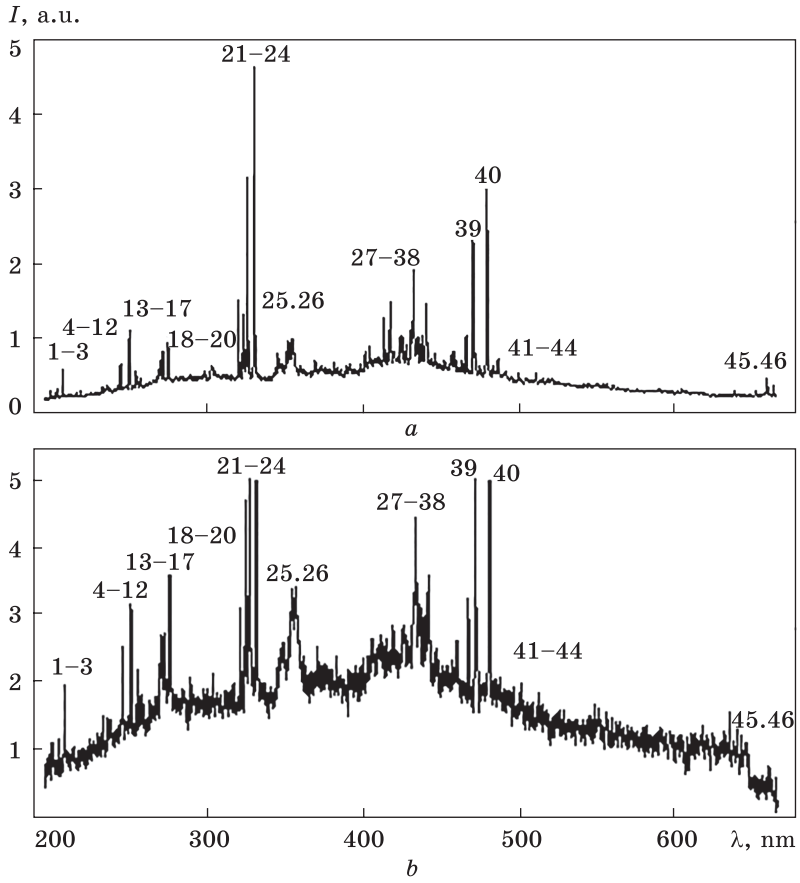

Fig. 12. Plasma emission spectra of the OND between the copper and zinc electrodes at p_{Ar} = 50 (*a*), 200 (*b*) kPa [32]

Investigation of the conditions for the synthesis of bipolar Cu–Zn nanostructures from the destruction products of zinc and copper electrodes in an OND of atmospheric pressure in inert gases is practically absent. Therefore, the problem of establishing the conditions for the deposition of thin composite films based on transition metals (Cu, Zn, Cd, Fe, *etc.*), which is carried out without the use of expensive laser or high-vacuum equipment, is actual.

For a discharge in argon at a pressure of 50 kPa, the amplitude of the largest voltage drop on the electrodes was achieved at the initial stage of the discharge and was ≈±2–4 kV, for current, ±80–100 A, and for pulsed power, 0.8 MW, that provided an energy contribution to one discharge pulse into plasma ≈ 122.6 mJ. With an increase in argon pressure to 200 kPa, the voltage difference of different polarity in the initial phase of the discharge at τ = 10–30 ns reached 15 kV, and for the cur-

Table 5. **Results of identification of plasma emission spectra of an overstressed nanosecond discharge between a copper electrode and a zinc electrode at p_{Ar} = 50 and 200 kPa [32]**

No.	λ_{tabl}, nm	I_{exp}, a.u. P_{Ar} = = 50 kPa	I_{exp}, a.u. P_{Ar} = = 200 kPa	Object	Lower energy, eV	Upper energy, eV	Lower term	Upper term
1	202.54	0.3	1.13	Zn II	0.00	6.11	$3d^{10}4s\ ^2S_{1/2}$	$3d^{10}4p\ ^2P^\circ_{3/2}$
2	203.93	0.32	0.84	Zn II	7.77	13.85	$3d^9(^2D)4s^2\ ^2D_{5/2}$	$3d^9(^2D)4s4p(^3P^\circ)\ ^4D^\circ_{5/2}$
3	207.99	0.57	1.88	Zn II	14.23	20.19	$3d^9(^2D)4s4p(^3P^\circ)\ ^2D^\circ_{5/2}$	$3d^9(^3D)5s\ ^4D_{3/2}$
4	213.59	0.26	1	Cu II	2.72	8.52	$4s\ ^3D$	$4p\ ^3F^\circ$
5	216.50	0.23	0.94	Cu I	0.00	5.72	$4s\ ^2S$	$4p'\ ^2D^\circ$
6	217.49	0.25	0.94	Cu II	8.92	14.61	$4p\ ^1F^\circ$	$4d\ ^1G$
7	218.17	0.29	1	Cu I	0.00	5.68	$4s\ ^2S$	$4p'^2P^\circ$
8	226.30	0.25	1.10	Cu I	1.64	7.12	$4s^2\ ^2D$	$7p\ ^2P^\circ$
9	229.43	0.28	1.22	Cu II	2.83	8.23	$4s\ ^3D$	$4p\ ^3P^\circ$
10	230.31	0.34	1.23	Cu I	1.64	7.02	$4s^2\ ^2D$	$4p''\ ^2D^\circ$
11	236.98	0.35	1.47	Cu II	3.26	8.49	$4s\ ^1D$	$4p\ ^3F^\circ$
12	244.16	0.66	2.43	Cu I	0.00	5.08	$4s\ ^2S$	$4p'\ ^4P^\circ$
13	255.79	0.47	2.19	Zn II	6.11	10.96	$3d^{10}4p\ ^2P^\circ_{3/2}$	$3d^{10}5s\ ^2S_{1/2}$
14	258.24	0.47	1.83	Zn I	4.02	8.82	$3d^{10}4s4p\ ^3P^\circ_1$	$3d^{10}4s6d\ ^3D_2$
15	268.41	0.55	2.68	Zn I	4.02	8.64	$3d^{10}4s4p\ ^3P^\circ_1$	$3d^{10}4s7s\ ^3S_1$
16	271.24	0.69	2.77	Zn I	4.07	8.64	$3d^{10}4s4p\ ^3P^\circ_2$	$3d^{10}4s7s\ ^3S_1$
17	275.64	0.92	3.58	Zn I	4.00	8.50	$3d^{10}4s4p\ ^3P^\circ_0$	$3d^{10}4s5d\ ^3D_1$
18	282.43	0.47	1.93	Cu I	1.39	5.78	$4s^2\ ^2D$	$4p'\ ^2D^\circ$
19	299.73	0.56	1.91	Cu I	1.64	5.78	$4s^2\ ^2D$	$4p'\ ^2D^\circ$
20	303.61	0.62	2.15	Cu I	1.64	5.72	$4s^2\ ^2D$	$4p'\ ^2D^\circ$
21	320.82	1.5	3.08	Cu I	1.64	5.51	$4s^2\ ^2D$	$4p'\ ^4D^\circ$
22	324.31	1.31	4.59	Cu I	0	3.82	$4s\ ^2S$	$4p\ ^2P^\circ$
23	327.39	3.14	5	Cu I	0	3.39	$4s\ ^2S$	$4p\ ^2P^\circ$
24	330.25	4.61	5	Zn I	4.02	7.78	$3d^{10}4s4p\ ^3P^\circ_1$	$3d^{10}4s4d\ ^3D_2$
25	344.60	0.78	2.59	N_2	Second positive system $C^3\Pi_u^+ - B^3\Pi_g^+$ (4; 5)			
26	354.89	0.96	3.42	N_2	Second positive system $C^3\Pi_u^+ - B^3\Pi_g^+$ (3; 2)			
27	368.65	0.67	2.13	Cu II	8.49	11.85	$4p\ ^3F^\circ$	$4s^2\ ^1G$
28	373.78	0.62	2.24	Ar II	21.5	24.81	$4p'\ ^2D^o$	$4d'\ ^2F$
29	380.31	0.70	2.34	Ar II	21.50	24.76	$4p'\ ^2D^\circ$	$4d'\ ^2D$
30	402.26	0.83	2.42	Cu I	3.79	6.87	$4p\ ^2P^\circ$	$5d\ ^2D$
31	403.54	0.87	2.43	Ar II	18.43	21.5	$4s'\ ^2D$	$4p'\ ^2D^\circ$
32	417.18	1.48	2.81	Cu II	14.99	17.96	$5p\ ^3P^\circ$	$7s\ ^3D$
33	433.35	1.9	4.46	Ar I	11.83	14.69	$4s'\ [S]^\circ$	$5p'\ [S]$
34	440.09	1.43	3.59	Ar II	16.41	19.22	$3d\ ^4D$	$4p\ ^4P^\circ$
35	446.05	0.78	2.52	Ar II	16.44	19.22	$3d\ ^4D$	$4p\ ^4P^\circ$
36	457.93	0.79	2.63	Ar II	17.26	19.97	$4s\ ^2P$	$4p\ ^2S^\circ$
37	463.72	0.69	2	Ar II	18.45	21.13	$4s\ ^2D$	$4p\ ^2F^\circ$
38	465.79	1.04	3.25	Ar II	17.14	19.80	$4s\ ^2P$	$4p\ ^2P^\circ$
39	470.33	2.37	5	Ar II	21.67	24.31	$3d\ ^2P$	$4f(2)\ ^3P_1{}^o$
40	479.87	3.02	5	Ar I	13.08	15.66	$4p\ [2S]$	$12d\ [3S]$
41	487.62	0.73	1.89	Ar I	12.91	15.45	$4p\ [S]$	$7d\ [1S]$
42	500.68	0.53	2	Cu II	14.65	17.13	$4d\ ^1D$	$4f\ ^1F^\circ$
43	510.55	0.54	1.57	Cu I	1.39	3.82	$4s^2\ ^2D$	$4p\ ^2P^\circ$
44	511.82	0.4	1.84	Ar I	13.09	15.52	$4p\ [2S]$	$6d'\ [2S]^\circ$
45	636.95	0.3	1.13	Ar I	13.17	15.12	$4p\ [1S]$	$5d\ [S]$
46	656.29	0.47	0.74	H_α	13.08	14.95	$4p\ [2S]$	$4d'[S]^\circ$

rent, ±80–100 A. The maximum value of the electrical pulsed power reached 2.5 MW at t = 50 ns. The main energy contribution to the plasma was made during the first 100 ns from the moment of ignition of the discharge. The energy of one discharge pulse reached ≈373.8 MJ.

As for the discharge in argon between copper electrodes, for the discharge in argon at atmospheric pressure between copper and zinc electrodes in the emission spectrum (Fig. 12), an intense continuum was recorded in the wavelength range of 350–460 nm with a maximum at λ = 420 nm. The continuous spectrum of plasma radiation began to be recorded after a time interval Δt = 40 ns from the beginning of the discharge, when the intensity of the argon ion lines began to increase sharply [30].

In the emission spectra of the plasma of a gas–vapour mixture of argon and copper (Fig. 3) in the UV-wavelength range of 214–330 nm (lines 1–23, Table 5), emission was observed at the transitions of the atom and singly charged copper ion. The most intense ionic spectral line was the line with λ = 227.62 nm Cu II, and the atomic intense lines were the resonance spectral lines of the copper atom with λ = 324.75 and 327.39 nm Cu I, in which the lower energy level is the ground level. In the UV-radiation spectrum, bands of the second positive system of the nitrogen molecule were also observed, since, in these experiments, the discharge chamber was evacuated only up to a residual air pressure of ≈10 Pa. In the wavelength range of 360–659 nm, radiation was observed mainly at the transitions Ar I, Ar II, as well as an intense spectral line of the hydrogen atom (λ = 656.29 H_α), which is due to the residual air pressure in the chamber after it was pumped out by a foreline pump. An increase in argon pressure from 50 to 200 kPa led to an increase in the intensity of most of the spectral lines of copper and zinc by a factor of 2–4.

When the distance between the electrodes is 2 mm and a bipolar generator of high-voltage nanosecond pulses is used, one or several (with a strong overvoltage of the discharge gap) cathode spots are formed, moving one towards the other.

The broadening of the emission spectrum of copper and zinc vapour plasma to a more distant UV region (up to 202.54 nm) as compared to the copper vapour range increases the efficiency of automatic irradiation of the substrate and the nuclei of the composite film on the substrate with hard UV radiation from the discharge plasma. This is important for influencing it electrical and optical characteristics (formation of antireflection bands) [12, 13].

In Ref. [50], the results of a study of thin-film solar cells $CuIn_{1-x}Al_xSe_2$ (CIASe), which were prepared on the basis of a sequential process of selenization of metal layers of precursors, are presented. Polycrystalline CIAS thin films with a chalcopyrite structure were synthesized. The best solar cells based on CIASe have short-circuit current density (J_{sc}),

open circuit voltage (V_{oc}), fill factor (*FF*) and efficiency as follow: 29.3 mA/cm^2, 430 mV, 51, 1 and 6.5%, respectively, for a total relative aluminium content Al/(In + Al) equal 0.2. Comparison of these values with similar data for the device without aluminium showed a significant increase in their efficiency. These data confirmed a significant improvement of device efficiency due to an increase in the absorber band gap in quaternary alloys of the CIASe type. Therefore, it is important to develop new physical gas-discharge methods for the synthesis of quaternary chalcopyrite based on Cu, In, Al, and Se in the form of thin films, which can be realized using an overstressed nanosecond discharge between electrodes made of aluminium and the corresponding ternary chalcopyrite ($CuInSe_2$).

With increasing the argon pressure from 13.3 to 100 kPa in an OND between the aluminium-made electrode ternary chalcopyrite, the plasma resistance increased and the matching with the modulator of high-voltage bipolar pulses improved. In this case, the maximum voltage amplitude swing increased to 60 kV, and the duration of the main part of the voltage oscillogram was ≈100 ns. The maximum amplitude of the current pulse reached 180–200 A. The maximum value of the pulsed power of the discharge was observed in the first 130 ns from the moment of its ignition and was equal to 4 MW. Increasing the argon pressure from 13.3 to 100 kPa results in increasing the energy of an individual electric pulse from 46 to 423 mJ.

Control studies of the plasma emission spectra were carried out for an OND in argon between two aluminium electrodes (Fig. 9, *b*), as well as between two electrodes from the $CuInSe_2$ compound. At an argon pressure of 13.3 kPa, two groups of spectral lines of the aluminium atom prevailed in the emission spectrum of the discharge: 308.21, 309.27, 309.28, 394.40, 394.89, and 396.15 nm. The spectral lines were less intense: 415.85, 419.83, 420.06 nm Al I. The spectral lines 308.21 and 394.40 nm (resonant) have the lower energy level of the ground state of the aluminium atom, and the energies of their upper states are 4.02 and 3.14 eV, respectively. The spectral lines are 309.27, 309.28 nm Al I, ending in a low energy level of 0.014 eV. The upper energy levels for the lines 415.85, 419.83, 420.06 nm Al I are in the range of 14.499–14.529 eV, and the lower ones are in the energy range of 11.548–11.624 eV.

Figure 13, presents the emission spectrum of an overstressed nanosecond discharge between electrodes from chalcopyrite at an argon pressure of 100 kPa. The results of identification of the main spectral lines and bands of the decay products of the chalcopyrite molecule in plasma based on various buffer gases, as well as a thorough analysis of the emission spectra are given in Refs. [51–59]. However, the main feature of the spectrum shown in Fig. 13 should be noted. The most intense in the spectrum were the spectral lines of atoms and ions of copper and

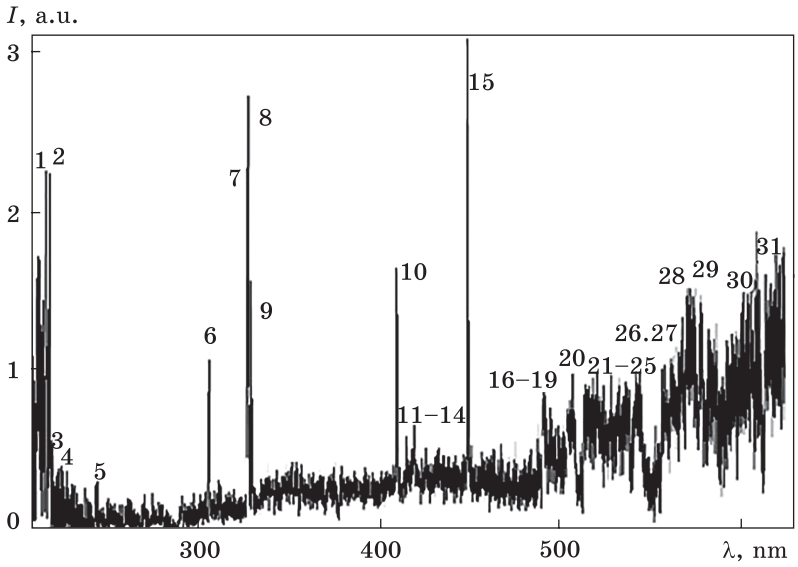

Fig. 13. Plasma emission spectrum of the OND between chalcopyrite electrodes at p_{Ar} = 100 kPa [32]

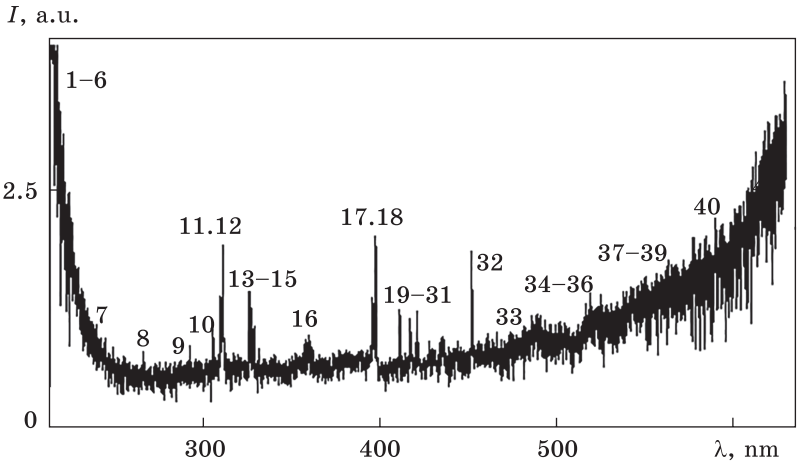

Fig. 14. Plasma emission spectrum of the OND between aluminium and chalcopyrite electrodes at the argon pressure of 100 kPa [32]

indium, which were observed against the background of continuous plasma radiation. Copper and indium atoms are less bound in the chalcopyrite molecule, which is the main component of massive electrodes [60]. Therefore, the linear part of the plasma emission spectrum is mainly caused by individual spectral lines of atoms and singly charged Cu and In ions. The emission spectrum of the gaseous component, argon, did not appear in this spectral region.

Table 6. **Results of identification of the most intense spectral lines of the atom and singly charged aluminium ion, as well as the molecular bands of the decay products of the chalcopyrite molecule in the OND at p_{Ar} = 100 kPa [32]**

No.	λ_{tabl}, nm	I_{exp}, a.u.	Object	Lower energy, eV	Upper energy, eV	Lower term	Upper term
1	214.89	3.90	Cu I	1.39	7.18	$4s^2\ ^2D$	$5f\ ^2F^\circ$
2	218.17	3.94	Cu I	0.00	5.68	$4s\ ^2S$	$4p'\ ^2P^\circ$
3	219.56	3.29	Cu II	8.78	14.43	$4p\ ^3D^\circ$	$4d\ ^3F$
4	219.95	2.88	Cu I	1.39	7.02	$4s^2\ ^2D$	$4p''\ ^2D^\circ$
5	221.45	2.40	Cu I	1.39	6.98	$4s^2\ ^2D$	$4p''\ ^2P^\circ$
6	224.20	2.45	Cu II	3.0	8.49	$4p$	3D
7	239.07	1.07	Al II	13.07	18.26	$4p\ ^3P^\circ$	$10d\ ^3D$
8	261.83	0.79	Cu I	1.39	6.12	$4s^2\ ^2D$	$5p\ ^2P^\circ$
9	284.02	0.68	Al I	4.02	8.39	$3d\ ^2D$	$3d\ ^2D^\circ$
10	306.34	0.92	Cu I	1.64	5.68	$4s^2\ ^2D$	$4p'\ ^2P^\circ$
11	308.21	1.34	Al I	0.00	4.02	$3p\ ^2P^\circ$	$3d\ ^2D$
12	309.27	1.88	Al I	0.01	4.02	$3p\ ^2P^\circ$	$3d\ ^2D$
13	324.75	1.42	Cu I	0	3.82	$4s\ ^2S$	$4p\ ^2P^\circ$
14	327.39	1.43	Cu I	0	3.39	$4s\ ^2S$	$4p\ ^2P^\circ$
15	329.05	1.05	Cu I	5.07	8.84	$4p'\ ^4F^\circ$	$4d'\ ^4F$
16	360.65	0.97	Ar I	11.62	15.06	$4s$ [S]°	$6p$ [S]
17	394.40	1.27	Al I	0.00	3.14	$3p\ ^2P^\circ$	$4s\ ^2S$
18	396.15	1.76	Al I	0.01	3.14	$3p\ ^2P^\circ$	$4s\ ^2S$
19	402.26	0.64	Cu I	3.79	6.87	$4p\ ^2P^\circ$	$5d\ ^2D$
20	405.67	0.70	Al II	15.47	18.52	$3s4d\ ^1D$	$3s15p\ ^1P^\circ$
21	410.17	1.19	In I	—	3.02	$5s^25p\ ^2P^\circ$	$5s^26s\ ^2S_{1/2}$
22	415.85	1.18	Ar I	11.55	14.53	$4s$ [S]°	$5p$ [1S]
23	417.83	1.12	Ar II	16.64	19.61	$4s\ ^4P$	$4p\ ^4D^\circ$
24	419.07	0.74	Ar I	11.55	14.51	$4s$ [S]°	$5p$ [2S]
25	420.06	0.90	Ar I	11.55	14.50	$4s$ [S]°	$5p$ [2S]
26	422.26	1.22	Ar II	19.87	22.80	$4p\ ^2P^\circ$	$5s\ ^2P$
27	425.93	0.73	Ar I	11.83	14.74	$4s'$ [S]°	$5p'$ [S]
28	426.62	0.70	Ar I	11.62	14.53	$4s$ [S]°	$5p$ [1S]
29	427.21	0.76	Ar I	11.62	14.52	$4s$ [S]°	$5p$ [1S]
30	430.01	0.76	Ar I	11.62	14.51	$4s'$ [S]°	$5p$ [2S]
31	433.35	0.89	Ar I	11.83	14.69	$4s'$ [S]°	$5p'$ [1S]
32	451.13	1.65	In I	0.27	3.02	$5s^25p\ ^2P^\circ$	$5s^26s\ ^2S_{1/2}$
33	484.22	1.18	Cu I	5.24	7.80	$4p'\ 4F^\circ$	$5s'\ 4D$
34	515.83	1.32	Cu I	5.69	8.09	$4p'\ ^2P^\circ$	$5s'\ ^2D$
35	516.22	1.13	Ar I	12.91	15.31	$4p$ [S]	$6d$ [S]°
36	518.77	1.42	Ar I	12.91	15.30	$4p$ [S]	$5d'$ [1S]°
37	549.58	1.57	Ar I	13.08	15.33	$4p$ [2S]	$6d$ [3S]°
38	555.87	1.46	Ar I	12.91	15.14	$4p$ [S]	$5d$ [1S]°
39	556.69	1.45	Se II	—	—	—	—
40	594.92	2.00	Ar I	13.28	15.35	$4p'$ [1S]	$6d$ [1S]
41	603.21	2.25	Ar I	13.08	15.13	$4p$ [2S]	$5d$ [3S]°

Table 7. **Results of identification of the most intense spectral lines of the atom and singly charged aluminium ion, as well as the molecular bands of the decay products of the chalcopyrite molecule in the OND at p_{Ar} = 13.3 kPa [32]**

No.	λ_{tabl}, nm	I_{exp}, a.u.	Object	Lower energy, eV	Upper energy, eV	Lower term	Upper term
1	214.89	1.09	Cu I	1.39	7.18	$4s^2\ ^2D$	$5f\ ^2F^\circ$
2	218.17	0.47	Cu I	0.00	5.68	$4s\ ^2S$	$4p'\ ^2P^\circ$
3	219.56	0.53	Cu II	8.78	14.43	$4p\ ^3D^\circ$	$4d\ ^3F$
4	219.95	0.55	Cu I	1.39	7.02	$4s^2\ ^2D$	$4p''\ ^2D^\circ$
5	221.45	0.57	Cu I	1.39	6.98	$4s^2\ ^2D$	$4p''\ ^2P^\circ$
6	224.20	0.49	Cu II	3.0	8.49	$4p$	3D
7	239.07	0.82	Al II	13.07	8.78	$4p\ ^3P^\circ$	$10d\ ^3D$
8	261.83	0.44	Cu I	1.39	6.12	$4s^2\ ^2D$	$5p\ ^2P^o$
9	284.02	0.27	Al I	4.02	8.39	$3d\ ^2D$	$3d\ ^2D^o$
10	306.34	0.71	Cu I	1.64	5.68	$4s^2\ ^2D$	$4p'\ ^2P^o$
11	308.21	2.08	Al I	0.00	4.02	$3p\ ^2P^\circ$	$3d\ ^2D$
12	309.27	3.02	Al I	0.01	4.02	$3p\ ^2P^\circ$	$3d\ ^2D$
13	324.75	1.38	Cu I	0	3.82	$4s\ ^2S$	$4p\ ^2P^\circ$
14	327.39	1.04	Cu I	0	3.39	$4s\ ^2S$	$4p\ ^2P^\circ$
15	329.05	0.79	Cu I	5.07	8.84	$4p'\ ^4F^\circ$	$4d'\ ^4F$
16	360.65	0.64	Ar I	11.62	15.06	$4s$ [S]°	$6p$ [S]
17	394.40	2.54	Al I	0.00	3.14	$3p\ ^2P^\circ$	$4s\ ^2S$
18	396.15	2.55	Al I	0.01	3.14	$3p\ ^2P^\circ$	$4s\ ^2S$
19	402.26	0.34	Cu I	3.79	6.87	$4p\ ^2P^\circ$	$5d\ ^2D$
20	405.67	0.58	Al II	15.47	18.52	$3s4d\ ^1D$	$3s15p\ ^1P^\circ$
21	410.17	1.01	In I	—	3.02	$5s^25p\ ^2P^\circ$	$5s^26s\ ^2S_{1/2}$
22	415.85	1.26	Ar I	11.55	14.53	$4s$ [S]°	$5p$ [1S]
23	417.83	0.5	Ar II	16.64	19.61	$4s\ ^4P$	$4p\ ^4D^\circ$
24	419.07	0.78	Ar I	11.55	14.51	$4s$ [S]°	$5p$ [2S]
25	420.06	1.51	Ar I	11.55	14.50	$4s$ [S]°	$5p$ [2S]
26	422.26	0.44	Ar II	19.87	22.80	$4p\ ^2P^\circ$	$5s\ ^2P$
27	425.93	0.73	Ar I	11.83	14.74	$4s'$ [S]°	$5p'$ [S]
28	426.62	0.61	Ar I	11.62	14.53	$4s$ [S]°	$5p$ [1S]
29	427.21	0.72	Ar I	11.62	14.52	$4s$ [S]°	$5p$ [1S]
30	430.01	0.62	Ar I	11.62	14.51	$4s'$ [S]°	$5p$ [2S]
31	433.35	0.81	Ar I	11.83	14.69	$4s'$ [S]°	$5p'$ [1S]
32	451.13	1.51	In I	0.27	3.02	$5s^25p\ ^2P^\circ$	$5s^26s\ ^2S_{1/2}$
33	484.22	1.12	Cu I	5.24	7.80	$4p'\ 4F^\circ$	$5s'\ 4D$
34	515.83	0.49	Cu I	5.69	8.09	$4p'\ ^2P^\circ$	$5s'\ ^2D$
35	516.22	0.53	Ar I	12.91	15.31	$4p$ [S]	$6d$ [S]°
36	518.77	0.50	Ar I	12.91	15.30	$4p$ [S]	$5d'$ [1S]°
37	549.58	0.65	Ar I	13.08	15.33	$4p$ [2S]	$6d$ [3S]°
38	555.87	0.62	Ar I	12.91	15.14	$4p$ [S]	$5d$ [1S]°
39	556.69	0.60	Se II	—	—	—	—
40	594.92	0.93	Ar I	13.28	15.35	$4p'$ [1S]	$6d$ [1S]
41	603.21	1.32	Ar I	13.08	15.13	$4p$ [2S]	$5d$ [3S]°

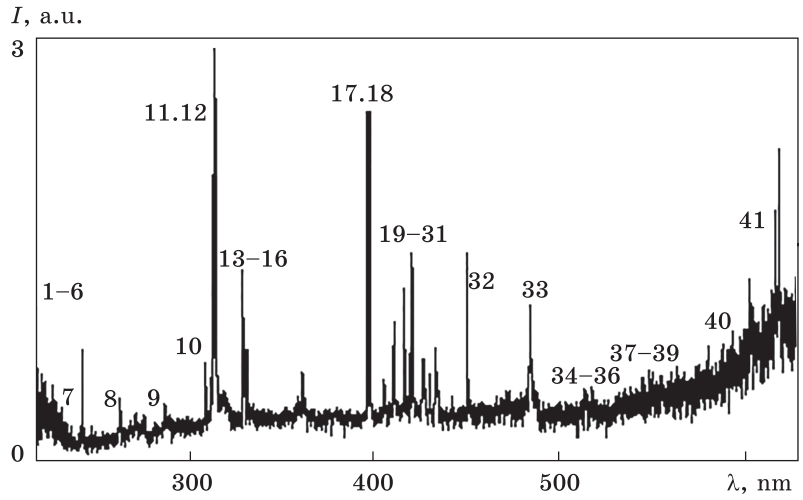

Fig. 15. Plasma emission spectrum of the OND between aluminium and chalcopyrite electrodes at the argon pressure of 13.3 kPa [32]

The emission spectra and the results of the identification of the most intense spectral lines of the atom and singly charged Al ion, as well as the molecular bands of the decay products of the chalcopyrite molecule in the OND between the Al-made electrode and chalcopyrite (at p_{Ar} = 101 and 13.3 kPa) are shown in Figs. 14 and 15, Tables 6 and 7.

At an argon pressure of 100 kPa, in the plasma emission spectrum based on a mixture of aluminium and chalcopyrite vapour, the shortest-wavelength and most intense part of the spectrum (lines 1–10) were represented by spectral lines of atoms and singly charged ions of copper and aluminium. The spectral lines were closely located in the background of the continuum and actually formed a certain band with a base length of 50 nm (from 200 to 250 nm).

The second group of spectral lines, which were also observed against the background of continuous radiation in the spectral range of 308–451 nm, had a higher degree of separation, but their intensities were low. In addition to atoms and singly charged ions of copper and aluminium, separate lines of Ar I, Ar II were also observed in the violet and blue regions of the spectrum. Only the atomic spectral lines 410.17 and 451.13 nm of In I appeared in the emission from indium lines.

In the spectral range of 450–650 nm, the intensity of continuous radiation strongly increased with increasing radiation wavelength. Against the background of continuous radiation, the spectral lines of the argon and copper atoms were mainly observed. The main reason for the appearance of an intense continuum in the spectrum is the transition of the diffuse form of an OND into a contracted state (spark) at atmospheric pressure of argon.

A decrease in the argon pressure to 13.3 kPa promoted the ignition of the discharge in a diffuse form, and the contraction was much less pronounced. This led to a better manifestation in the emission of individual spectral lines of atoms and singly charged ions of copper, aluminium and argon (Fig. 15). The intensity of the group of spectral lines of copper and aluminium in the wavelength range of 200–225 nm (lines 1–6) decreased four times. At a reduced argon pressure, the most intense and well-separated spectral lines (7–18) from the wavelength range of 230–400 nm. The intensity of continuous radiation in this spectral range was minimal. Here, the most intense were the spectral lines (11, 12, 17, 18): 308.21 (resonance line) 309.27, 394.40, 396.15 nm Al I. Other spectral lines from this spectral interval belonged mainly to copper and aluminium atoms.

The next rather well separated group of spectral lines (19–33) was emitted in the wavelength range of 400–500 nm. It was represented by the spectral lines of the atom and singly charged argon ion and the spectral lines of 451.13 nm In I, 484.22 nm, 515.83 nm Cu I.

In the spectral range of 500–630 nm, continuous radiation (probably thermal radiation of the plasma) prevailed, against the background of which, the spectral lines 594.92 nm and 603.21 nm Ar I were distinguished.

With an increase in the argon pressure from 13.3 to 100 kPa, the intensities of the spectral lines of copper and indium atoms and their singly charged ions increased. Thus, the maximum increase was found for the intensity of the 218.17 nm Cu I spectral line (by a factor of 8.6), the lower for which is the main energy level of the copper atom, and for the 219.56 nm Cu I ion line, an increase in intensity was recorded by 6.3 times. For the resonance line of the copper atom at 306.34 nm, probably due to self-absorption of radiation in the plasma, the increase in intensity was small (only about 1.3 times). An increase in the intensity of the lines of the indium atom 410.17, and 451.22 nm was also small (circa 1.1–1.2 times).

For the intensity of the spectral lines of the aluminium atom 308.21, 309.27, 394.40 (resonance line), 396.15 nm with an increase in argon pressure, a decrease in intensity was observed (Tables 1, 2) from 1.4 to 2.3 times. For the ionic lines of aluminium, 239.07 and 405.67 nm of Al II, with an increase in argon pressure, an increase in intensity was recorded (about 1.3 times; Tables 1, 2). For the intensities of the spectral lines of the argon atom at 549.58 and 594.92 nm, with an increase in its pressure, the greatest increase in the intensity was obtained (2.4 and 2.2 times, respectively; Tables 6, 7). For the argon ionic lines at 417.83 and 422.26 nm of Ar II, the increase in intensity was 2.3 and 2.8 times, respectively (Tables 1, 2).

Based on the spike structure of current pulses, the processes of stepwise excitation and stepwise ionization through the corresponding

metastable states typical of high-current high-pressure discharges can also be important [61]. Therefore, a likely mechanism for the formation of doubly charged ions of copper, aluminium, and argon in the ground energy state can be direct and stepwise excitation of the corresponding singly charged ions by electron impact and the processes of dielectronic recombination of two and singly charged ions with plasma electrons.

An increase in the argon pressure promotes an increase in the intensity of the spectral lines of Cu and In atoms and their singly charged ions due to an increase in the efficiency of the recombination mechanism at high pressures of the buffer gas [61], as well as in the processes of stepwise excitation and ionization of the corresponding atoms with an increase in the energy contributions to the plasma at an argon pressure at the level of 100 kPa. The main feature of the introduction of copper and indium vapours into the plasma is the dissociation reaction of the chalcopyrite molecule, and the formation of excited atoms and singly charged aluminium and argon ions in the processes of stepwise electronic excitation and ionization followed by dielectronic recombination.

Aluminium in relation to argon and chalcopyrite molecules is an easily excited and easily ionized element of the studied plasma. Therefore, with a high probability, singly and doubly charged ions, primarily of Al, can be formed directly in the process of microexplosions of natural inhomogeneities on the surface of an aluminium electrode [8].

3.3. Energy Characteristics

Figures 16 and 17 present the results of optimization of the average intensity of the UV radiation of the discharge depending on the pulse repetition rate and on the value of the charging voltage across the working capacitor of the high-voltage modulator (Fig. 16).

The maximum values of the average power of UV radiation in argon at an argon pressure of 101 kPa for various UV ranges were as follow: for UV-C (200–280 nm), 67 mW/m^2, for UV-B (280–315 nm), 65 mW/m^2, and for UV-A (315–400 nm), 204 mW/m^2 (at U_{ch} = 20 kV, f = 1 kHz). With a decrease in argon pressure to 6.7 kPa, the maximum value of the average power of UV radiation in the UV-C spectral range (200–280 nm) became 4.4 W/m^2, in the UV-B (280–315 nm) range, 4.4 mW/m^2, and in the UV-A (315–400 nm) range, 11.7 mW/m^2 (at U_{ch} = 20 kV, f = 1 kHz).

With an increase in the pulse repetition rate from 40 to 1000 Hz, the largest increase in the discharge radiation intensity in the UV-A (315–400 nm) range, in particular, in the frequency range Δf = 350–1000 Hz, it increased from 8 to 95 mW/m^2. In the UV-B, UV-C ranges, the increase in the radiation power density was less and was observed in the range of 3.0–25.0 mW/m^2. The increase in the intensity of UV ra-

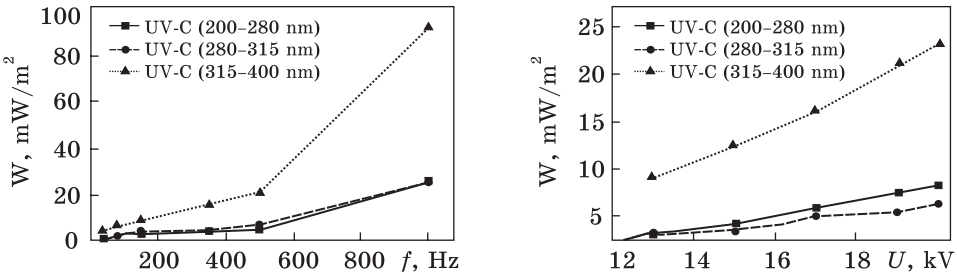

Fig. 16. The intensity of UV radiation (UV-C, UV-B, UV-A ranges) of high-voltage nanosecond discharge vs. the repetition rate of voltage pulses at a charging voltage U = 13 kV (f = 80 Hz, p_{Ar} = 100 kPa, d = 2 mm) [32]

Fig. 17. The dependence of the intensity of UV radiation (UV-C, UV-B, UV-A ranges) of high-voltage nanosecond discharge on the value of the charging voltage on the working capacitor of the high-voltage modulator (f = 80 Hz, p_{Ar} = 100 kPa, d = 2 mm [32]

diation of the discharge, depending on the value of the charging voltage on the working capacitor of the high-voltage modulator at a fixed repetition rate, was less effective and was in the range of 8.0–24 mW/m^2. In this case, the relative ratios between the intensities of radiation in the ranges of UV-C, UV-B, UV-A were the same as for the corresponding dependences on frequency.

Figure 18 presents the dependences of the average power of UV radiation of an overstressed bipolar nanosecond discharge between copper electrodes in air at atmospheric pressure in the spectral range of 200–280 nm on the voltage pulse repetition rate and the charging voltage of the working capacitor of the high-voltage modulator. The frequency dependency of the UV radiation power of a nanosecond discharge was nonlinear, its maximum increase was observed in the frequency range of 40–350 Hz. With an increase in the voltage-pulse repetition rate from 35 to 1000 Hz, the average power of the UV radiation of the discharge increased by about an order of magnitude. An increase in the charging voltage of the working capacitor from 13 to 20 kV (at f = 35 Hz) led to an increase in the UV-radiation power of the discharge only twofold. The results obtained show that to increase the average power of the UV radiation of the discharge, the most promising is to increase the repetition rate of voltage pulses.

The results of studying the UV radiation of zinc vapour plasma were also close to the results shown in Fig. 18.

A study of the energy characteristics of a multi-channel spark discharge [43] showed that it was ignited in the form of a set of successive microplasma formations with a specific energy contribution of 1 kJ/cm^3 and an electron concentration of 10^{17} cm^3. Plasma radiation was dominated by the radiation of atoms and ions of the material of the elec-

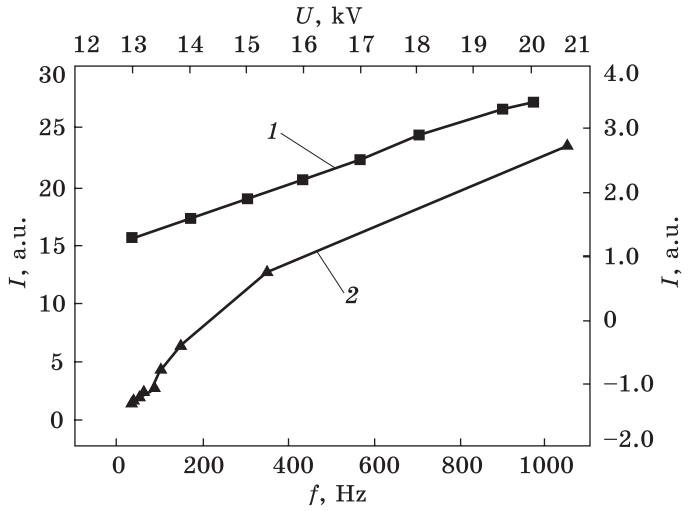

Fig. 18. The average radiation power of the discharge plasma in air between copper electrodes in the spectral range 200–280 nm *vs.* the (*1*) pulse repetition rate (at a fixed charging voltage of the working capacitor of the high-voltage modulator U = 13 kV, d = 0.001 m, f = 35 Hz, p = 101 kPa) and *vs.* the (*2*) value of the charging voltage of the working capacitor of the high-voltage modulator (at f = 35 Hz) [7]

trodes made of copper or stainless steel. The results of measuring the intensity of UV radiation from plasma, carried out by the actinometry method, showed that the efficiency of UV radiation relative to the energy introduced into the discharge reaches 1%, and the energy in a radiation pulse was ≈2 mJ.

4. Plasma Parameters

Let us consider the determination of the parameters of a high-voltage nanosecond discharge with copper electrodes at various air pressures based on the relative intensities measured in our experiment.

Using our radiation intensities at the transitions of atoms and ions, taking into account the relative spectral sensitivity of the experimental setup, as well as data on the decay times of excited states with different radiation channels, we calculated the relative populations of excited states of atoms and singly charged ions [62]:

$$\frac{N_j}{g_j} = \sum_k \frac{\lambda_{jk} I_{jk}}{A_{jk} g_j}, \qquad (1)$$

where λ is the radiation wavelength, A is the transition probability, I is the spectral line intensity, g is the statistical weight of the level, and the j, k subscripts denote the upper and lower levels of the emitting transition.

Using the populations of the excited states, the Boltzmann distribution was constructed in a linear form. The distribution of the natural logarithm for the population of excited states of atoms and ions with energies (E) makes it possible to analyse the features of the formation of excited states, estimate the ratio of the concentrations of atoms and ions, determine the temperature (T_e) and concentration (N_e) of electrons in the plasma, and draw conclusions regarding ionization equilibrium. Since possible nonradiative transitions within the closely spaced energy states lead to a redistribution of the population between them, additional statistical processing is required for them [61]. To determine the electron temperature, the best result was obtained by statistical processing of the levels, between which the energy gap was less than 0.2 eV. Working formula for calculations [63] is:

$$T_e = \frac{\Delta E}{\Delta \ln(N/g)}. \qquad (2)$$

The approximation of the experimental points by a linear dependence was carried out with a minimum sum of deviations. To determine the concentration of electrons using the Saha equation during statistical processing with $dE < 0.5$ eV, the working formula [63, 64] is:

$$n_e = 2\frac{I_2 A_1 g_1 \lambda_2}{I_1 A_2 g_2 \lambda_1} 6.0436 \cdot 10^{21} T_e^{3/2} \exp\left(-\frac{E_2 - E_1}{T_e}\right), \qquad (3)$$

where subscript 2 refers to ion, 1 to atom. Substituting the electron temperature and the energy of the upper level (in electron-volts, eV), we obtain the electron concentration in cm^{-3}. To determine the degree of plasma ionization and to determine the ionization equilibrium temperature, the values of the population of the ground state of atoms and ions were used after constructing the combined distribution of the population.

To calculate the plasma parameters at various air pressures, radiation spectra were obtained in the wavelength range of 200–650 nm. The identification of the spectra showed the presence of atoms and atomic ions of copper and nitrogen. The discharge is ignited in air, which results in the formation of ionized particles, causing the sputtering of copper electrodes. The main component of air is molecular nitrogen, and its dissociation and ionization occurs before sputtering and provides information about the destruction of electrodes, the energy characteristics of this process. That is why we mainly focus on the study of nitrogen radiation and the use of these data to estimate the parameters of the discharge plasma. Intensities of radiation of atoms and atomic ions of nitrogen at air pressures of 0.3–2 atmospheres are shown in Table 8 [32]. In Table 8, the following designations are made: λ is wavelength in

nanometers; E_{up} is the energy of the upper state in eV; J_b is principal quantum number; K_b is electronic configuration of the upper position; I is the radiation intensity in relative units (the voltage sensitivity of the photomultiplier, spectral sensitivity and zero shift due to heating during operation are taken into account), and the subscript means pressure in atmospheres.

After normalizing the intensity, the energy distribution of the population was plotted. The analysis was carried out separately for each element and the degree of its ionization using statistical data processing

Table 8. **Deciphering the emission spectrum of air plasma in the OND with copper electrodes at different air pressures (in terms of the decomposition products of the nitrogen molecule) [32]**

λ, nm	Object	E_{up}, eV	J_b	K_b	Term	I_2	I_1	$I_{0.7}$	$I_{0.3}$
333.0	N II	24.37	0	4*s*	3P°	48.1	60	80.1	61.7
343.7	N II	22.10	0	3*p*	1S	39.5	88.5	75.6	54
383.8	N II	24.39	2	4*s*	3P°	35.7	39.2	55.3	36.3
391.9	N II	23.57	1	3*d*	1P°	41.1	44.3	64.3	39.9
395.6	N II	21.60	2	3*p*	1D	41.7	40.4	58.8	33.1
399.5	N II	21.60	2	3*p*	1D	91.7	98.3	174	119.5
404.1	N II	28.22	2	7*s*	3P°	68.6	65.3	81.1	59
411.0	N I	13.71	2.5	3*p*	2D°	74.5	55.5	95.5	59.6
422.8	N II	24.53	1	4*s*	1P°	83.7	71.3	187.3	79.5
438.6	N I	14.95	1.5	3*d*	2S	105.7	48.1	71.2	61.7
444.7	N II	23.20	2	3*d*	1D°	97.1	66.5	94	85.4
463.1	N II	21.16	2	3*p*	3P	60.8	53.8	148.6	82.2
469.9	N II	30.37	0	3*d*	5D	29.3	26.5	50.4	34
478.8	N II	23.24	2	3*d*	3D°	22.8	22.3	29.5	21.2
480.3	N II	23.25	3	3*d*	3D°	26.6	26.2	39	24
500.5	N II	23.14	4	3*d*	3F°	65.4	68.3	188.7	145
517.6	N II	30.13	4	3*d*	5F	23.3	23.8	41.4	28.9
520.2	N I	13.99	1.5	5*d*	2P	21.2	19.4	22	15.3
548.0	N II	23.42	1	3*d*	3P°	12.3	16.1	15.2	12.6
552.0	N I	14.00	0.5	5*d*	4D	17.4	16.4	18.6	16.7
553.5	N II	27.75	4	3*p*	5D°	8.8	13.4	16	14.4
566.7	N II	20.65	2	3*p*	3D	18.5	25.3	56.8	44.4
568.0	N II	20.67	3	3*p*	3D	9.9	15.5	18.6	15.3
575.3	N I	14.00	3.5	5*d*	4D	11	15.2	14.2	11.6
590.0	N II	28.35	1	3*p*	3D°	6.1	15.2	21.6	21
591.0	N II	28.35	1	3*p*	3D°	4.8	16.4	17.1	18.9
593.2	N II	23.24	2	3*d*	3D°	3.4	14.3	13.7	13.5
648.2	N II	20.41	1	3*p*	1P	10.2	15.2	12.7	16.7
650.0	N I	13.66	2.5	4*d*	4F	29.8	22.3	38.5	23.1
655.4	N II	25.13	1	4*p*	3D	—	20	25.6	19.4
662.3	N I	13.63	2.5	5*s*	4P	—	14.6	14.7	—

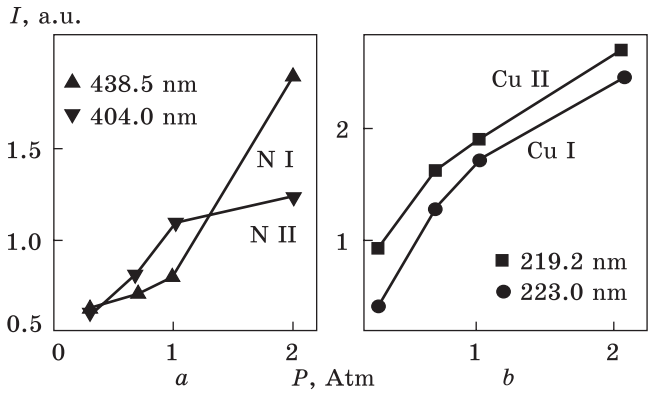

Fig. 19. The radiation intensity of Cu and N atoms and ions *vs.* the pressure. For intense copper lines, an increase was observed with a transition to saturation [32]

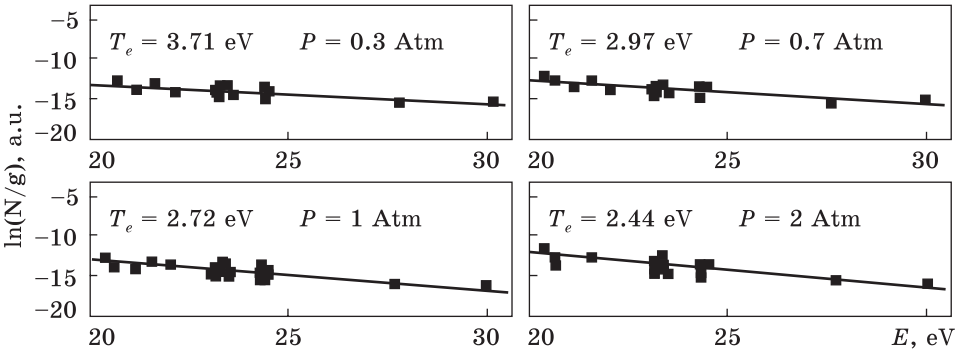

Fig. 20. Population distribution of excited states of singly charged nitrogen ions [32]

for levels, the energy gap between which is less than 0.2 eV. In the selected pressure range, the radiation of atoms and atomic ions in the time-averaged spectra was much more intense from the radiation of molecules. A typical change in intensity with a change in air pressure is shown in Fig. 19.

The increase in pressure contributed to a better energy contribution and radiation manifestation. For nitrogen, up to a pressure of 1 atmosphere, a rapid growth dominates for the emission of ions, and after, for atoms. It is possible to assume that an increase in air pressure improves the process of sputtering of electrodes, redistribution of energy between plasma components, and contributes to a greater efficiency of recombination processes. The distribution of the population of the excited states of nitrogen ions clearly indicates a thermal nature and makes it possible to determine unambiguously the electron temperature, which is shown in Fig. 20.

The generalized data in Fig. 20, together with the overlapping of the population distribution for atoms and ions, makes it possible to estimate the electron concentration and the degree of ionization of atomic

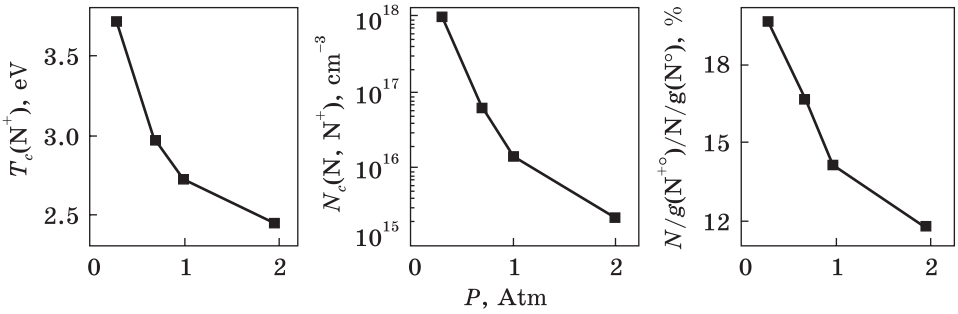

Fig. 21. Pressure-dependent electron temperature (left) and concentration (middle) along with degree of nitrogen ionization (right) [32]

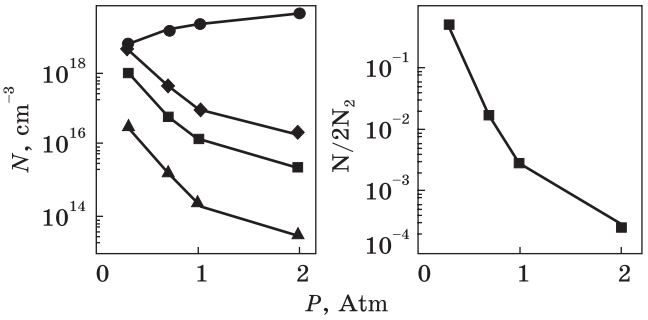

Fig. 22. Pressure-dependent concentrations of atoms, molecules, and atomic ions of nitrogen (left) and degree of dissociation of nitrogen molecules (right) [32]

nitrogen from the ratio of the population of the ground states of atoms and ions.

From Figure 21, it follows that an increase in air pressure leads to a sharp decrease in the degree of nitrogen ionization from 19.5 to 11.5%. The electron concentration decreases by three orders of magnitude (10^{18}–10^{15} cm^{-3}), and the temperature decreases from 3.7 to 2.4 eV. The ionization energy of nitrogen atoms is 14.53 eV.

Ionization equilibrium, according to the combined distribution of the population of nitrogen atoms and ions, corresponds to a temperature close to the ionization energy of copper (7.72 eV). Having the relative ratios of the population of atoms, one and two charged ions, the absolute values of the temperature and concentration of electrons, using the ratio of molecular physics, we can make estimates of the absolute values of the concentrations of atoms, molecules, atomic ions, and determine the degree of dissociation of nitrogen molecules at different pressures. These values are shown in Fig. 22.

The concentration of singly charged ions of atomic nitrogen with increasing pressure decreases in the range of 10^{18}–10^{15} cm^{-3}. The concentration of doubly charged ions at a pressure of 0.3 atmospheres reaches a value of more than 10^{16} cm^{-3}; however, at a pressure of two atmospheres, it drops to 10^{13} cm^{-3}. The concentration of molecules be-

fore breakdown with a change in pressure is in the vicinity of 10^{19} cm^{-3}, and the concentration of atoms in the discharge decreases from $4 \cdot 10^{18}$ to $2 \cdot 10^{16}$ cm^{-3} with increasing pressure. The degree of dissociation of molecules with an increase in pressure from 0.3 to 2 atm drops sharply from 0.5 to $2 \cdot 10^{-4}$. With a small change in the concentration of molecules with pressure (within one order of magnitude), this behaviour indicates the presence of features of processes in plasma with the participation of molecules, which are interesting for study, but due to the weak manifestation of molecular radiation in the integral spectra, it requires additional experimental approaches. Generally, judging by the emission of the atomic component, nitrogen is best manifested in the form of excited states of ions and highly excited energy states of atoms, probably due to associative-dissociative processes involving atoms in the ground state, molecules and their ions.

Based on the experimentally measured spectral characteristics of air plasma in an overstressed nanosecond discharge between copper electrodes (in terms of the relative intensity of spectral lines of nitrogen atoms), the temperature and concentration of electrons in the plasma are calculated. This made it possible to judge the energy aspects of the sputtering of copper electrodes, the typical concentrations of the atomic and ionic components of the plasma, as well as the possible influence of chemical processes in the technological application of this type of discharge in air.

The process of plasma expansion of the cathode spot and the formation of shock waves at the stage of formation and development of a pulsed volume discharge in argon at atmospheric pressure was studied using the emission spectra of the near-cathode plasma and the space-time patterns of the development of the glowing body in [29–31]. Analytical expressions were obtained for calculating the radius of the cathode spot plasma and the rate of its expansion, which were in satisfactory agreement with the experimental results. Microexplosions on the electrode surface initiate the transition from volumetric to spark discharge in high-pressure gases. This leads to local heating of the cathode and plasma expansion with a velocity of $\approx 10^6$ cm/s. In this case, a shock wave propagates in the weakly ionized discharge plasma. For a spark channel that expands, a stage with a supersonic speed and a stage with a subsonic speed are distinguished, when the shock wave front breaks away from the boundary of the spark channel. The first stage lasts hundreds of nanoseconds, during which a shock wave is formed. The intensity of the latter is determined by the rate at which energy is introduced into the discharge. Volumetric discharges collide into a spark due to the development of near-electrode instabilities. After applying a voltage pulse with amplitude greater than the amplitude of the static breakdown in the pre-ionized gap, a weak diffuse glow with a diameter

of 0.5 cm appears along its anode after a time of 250 ns, propagating towards the cathode at a speed of $\approx 10^7$ cm/s. As the ionization of the front toward the cathode developed, the intensity of this glow increased and the cathode region was closed by a narrow ($d \approx 0.2$ mm) filamentary glow. The diameter of the diffuse channel at this stage was 4 mm, and after 20–25 ns, a cathode spot was formed on the cathode. In this case, the discharge took the form of a cone with apex at the cathode.

The cathode region was clearly outlined by a boundary with a diameter of $d = 0.2$–0.3 mm. The cathode spot was formed simultaneously with the onset of a sharp increase in current and a drop in voltage across the gap (the resistance of the gap between the electrodes when the cathode region was closed was 1 kΩ). At the initial stages of formation of the cathode spot, it was hemispherical with an expansion rate of $\approx 2.5 \cdot 10^6$ cm/s. The explosive-simulation model of formation of a cathode spot is based on the introduction of significant energy at the micropoints of the cathode surface, followed by their heating and explosion. The current density in the spark channel formed after a time $\tau = 30$–40 ns from the beginning of the discharge reaches 10^6 A/cm^2. At the same time, the rate of growth of the spark channel from the cathode spot increased almost linearly from 1.3 to $5.5 \cdot 10^6$ cm/s with an increase in the current density within $(1–9) \cdot 10^5$ A/cm^2. When a large number of cathode spots are formed in the discharge, many parallel plasma channels are observed, which at the initial stages of the discharge merge with each other and form a homogeneous plasma column with high conductivity. With the formation of the cathode spot, the radiation spectrum of the near-cathode plasma was characterized by intense lines of the cathode material, namely, Al I 396.1, 394.4, 280.1, 281.6 nm, and an intense continuum was recorded in the 260–360 nm region of the spectrum. The emission intensity of Al I spectral lines reached a maximum after 20–30 ns, and the intensity of the continuum was the highest at $\lambda = 420$ nm. The temperature of the cathode plasma was estimated from the relative radiation intensity of the spectral lines of argon, after a time $\tau = 30$–40 ns, was of 4–5 eV, and the temperature of electrons in the diffuse channel, which was tied to the cathode spot, was 1 eV. A spark channel grew from the cathode spot towards the anode.

At the initial stage of the cathode spot development (at $\tau = 20$–30 ns), the electron concentration in the diffuse channel was 10^{15}–10^{16} cm^{-3}. According to modern concepts, the emission of electrons from a microtip on the cathode surface (at a sufficiently large near-cathode potential drop before its explosion) lasts a time $t = 1$–10 ns. Therefore, the process that determines the duration of the uniform burning of the discharge is the formation of a near-cathode potential drop ($E \approx 10^5$ V/cm). The process of the formation of a cathode spot at the beginning of its development includes the stage of heating the metal in a solid state,

melting it, and heating the liquid metal until the beginning of vaporization. At this stage, the density of the metal is considered constant. The second stage corresponding to an explosion is characterized by a sharp increase in the resistance of the conductor and is difficult for quantitative research.

For comparison, the plasma temperatures of the spark channel in argon were estimated at various strengths of the external magnetic field H. T_e was determined by the method of relative radiation intensities (Orshtein's method), from three pairs of spectral lines Ar I: 448.2 and 454.5 nm, 480.6 and 476.4 nm, 484.74 and 476.4 nm. The electron temperature decreased during the time interval $\tau = 10–300$ ns. When the strength of the external magnetic field $H = 0$, the value of T_e decreased from 4.2 to 3.4 eV during the time interval $\tau = 100–500$ ns. The explosive nature of the formation of the cathode spot during the release of plasma energy is confirmed by the fact that the radial expansion of the cathode spot plasma stops very quickly. Comparison of the expansion rates of the cathode spot in argon and air showed that the expansion rate in air at the same energy inputs is much lower than the expansion rate of the cathode spot in argon. This indicates that the decay of the shock wave that carries the ionization front in air occurs faster in argon. Unlike argon in air, the shock wave energy is additionally spent on the dissociation of molecules. Since the bulk of the energy is introduced into the cathode spot in the plasma phase, a plasma bunch expands, in which energy is introduced into the substance by heating the electronic component with the subsequent transfer of energy from electrons to ions. The obtained speeds of movement at the level of $2 \cdot 10^6$ cm/s correspond to a kinetic energy of 50–100 eV. According to the explosive mechanism of the formation of the cathode spot, an 'ecton' is formed, which has the number of electrons of $10^{11}–10^{12}$, and the metal clot that evaporates can be positively charged. Therefore, the electrostatic field will additionally accelerate the ionic component of the plasma. At the initial stage of the discharge of the expansion of the cathode spot, its radius was $\approx 10^{-6}$ m. With an external magnetic field $H = 0$, the radius of the cathode spot increased in the range $(0.5–4.3) \cdot 10^{-4}$ cm with increasing time t from 5 to 50 ns.

The results of an experimental study of the emitting and spectral characteristics of a spark channel in argon at atmospheric pressure, both in a magnetic field and without it, are presented in Refs. [30, 31]. It was found that the imposition of a magnetic field significantly changes the distribution of the discharge radiation intensity (meanwhile, the magnetic field is an effective tool for manipulating charge transfer in materials [65–67]). The channel stage of the spark discharge in high-pressure gases is characterized by the maximum glow brightness. However, for the construction of a theory of a spark discharge and the de-

velopment of appropriate radiation sources, it is important to investigate the plasma parameters and physical conditions in the plasma of the spark discharge channel. Early studies of this kind showed that the average gas density in the spark channel at the later stages of development is $5 \cdot 10^{-6}$ g/cm^3, which corresponds to a concentration of $\approx 10^{17}$ cm^{-3}. In this case, the average temperature of the plasma in the channel reached $40 \cdot 10^4$ K. The constancy of the temperature in the spark channel was carried out over a wide range of changes in the rate of energy input into the plasma. From this, it was concluded that the saturation of the brightness of the spark channel radiation is limited by the plasma temperature inside the plasma channel. The spectrum of the pre-spark diffuse channel included mainly intense spectral lines Ar I: 442.3, 436.3, 433.5, 355.6 nm. The broadening of these spectral lines at this stage of the discharge was small (0.05–0.1 nm) and corresponded to an electron concentration of about 10^{16} cm^{-3}. In the early stages of the discharge, some ionic lines were also intensely excited, namely, Ar II: 372.9, 358.8, 354.5 nm, which have excitation energies of 19.96, 22.94, 24.62 eV, respectively, as well as an intense continuum in the spectral range of 350–460 nm with a maximum at $\lambda = 420$ nm. Over a period, the brightness of the ion lines increased, and a continuous spectrum began to be recorded. The maximum brightness of the ionic lines and the continuous spectrum was reached in a time of 300–400 ns from the beginning of the sharp increase in the current. The electrode material (Al) was represented by spectral lines of 289.1, 281.6 nm Al I. Relative intensity of the spectral lines of the argon atom: 480.6, 454.5, 422.8 nm in the absence of a magnetic field were 10, 3.39, 2.51 relative units, respectively, for time $t = 300$ ns.

To determine the temperature of the electrons in the spark channel, we used the method of relative intensities of spectral lines. The following Ar II lines were chosen: 448.18, 454.5, 480.6, 476.4, 484.7 nm. For these lines of the argon ion, the profile distortions due to self-absorption were insignificant. The optical thickness at $N_e \approx 10^{18}$ cm^{-3} and $kT = 3$ eV for $\lambda = 480.6$ nm is of 1 cm, which significantly dominated the characteristic dimensions of the spark channel. For the spectral line $\lambda = 480.6$ nm Ar II, the mode of local thermodynamic equilibrium is fulfilled for stationary plasma with $N_e \geq 10^{17}$ cm^{-3} and $kT = 3$ eV. For given plasma concentration, the equilibration time was 7 ns, and for $N_e \approx 10^{18}$ cm^{-3}, this time decreased to 1 ns. According to the criterion for an over-spark discharge, only partial local thermodynamic equilibrium (LTEE) is possible that was established in less than 10 ns and shown by the example of spectral lines of 480.6, 484.7 nm at $N_e \approx 10^{17}$ cm^{-3} and $kT = 3$ eV. Therefore, the value of the plasma temperature was determined for the instant of time 40 ns after the onset of a sharp increase in the current: $5.2 \cdot 10^4$ K. The time of equalization of the temperature

of electrons and ions in the plasma at $N_e \approx 10^{18}$ cm^{-3} was about 10 ns, and the average temperature of electrons determined from the relation of the intensities of the Ar II lines was of about 3.7 eV. At the stage of slow expansion of the spark channel, that is, starting from the moment of 500 ns, the intensity of continuous radiation decreased, as did the intensity of the argon ion lines. At the same time, the intensity of the lines Ar I: 394.9, 308.2 nm and lines Al II: 281.6, 289.1 nm was growing. In the absence of a magnetic field, the temperature of plasma electrons dropped rapidly (t = 1.5 μs; $T \approx 28 \cdot 10^3$ K), and in a magnetic field, the temperature drop slowed down (t = 1.5 μs; $T \approx 26 \cdot 10^3$ K). The maximum radiation energy in a magnetic field shifted the short-wavelength region of the spectrum, which was due to an increase in the plasma temperature. The width of the spectral lines at significant concentrations of charged particles in the plasma is determined by the Stark broadening. Thus, the half-width of the 480.6 nm line of Ar II at a current of 600 A (t = 300 ns) was of 0.42 nm that corresponded to an electron concentration of $2.4 \cdot 10^{18}$ cm^{-3}, and for the 422.8 nm line, the half-width was of 0.24 nm and $N_e \approx 2.1 \cdot 10^{18}$ cm^{-3}. That is, the electron concentrations determined from the half-widths of various Ar II lines turned out to be close.

5. Nanotechnological Application of the OND

Synthesizing nanostructures of transition metal oxides using a glow discharge with a liquid non-metallic electrode in air at atmospheric pressure [64] or also a high-voltage discharge of nanosecond duration [68, 69], a colloidal solution with the corresponding nanostructures is obtained, and not films or ultradispersed powders. Powders can be isolated from such solutions by evaporation, and the synthesis of thin nanostructured films is best performed in a high-voltage gas discharge between metal or semiconductor electrodes in a corresponding high-pressure gas medium.

The deposition of thin films was carried out for 0.5–2 hours with the installation of a glass substrate at a distance of 2–3 cm from the centre of the discharge and a gas pressure of 13–200 kPa and a distance between the electrodes of 1–3 mm.

The photoluminescence spectra of the synthesized films were studied by irradiating the film with a high-pressure mercury arc lamp in the wavelength range: 270–540 nm. In this case, the radiation of the mercury lamp in the spectral intervals of 5 nm stood out in the vicinity of the selected wavelengths nm using a monochromator and directed to the film surface. The photoluminescence spectrum of the nanostructures was recorded using another monochromator equipped with a separate photoelectric radiation detection system.

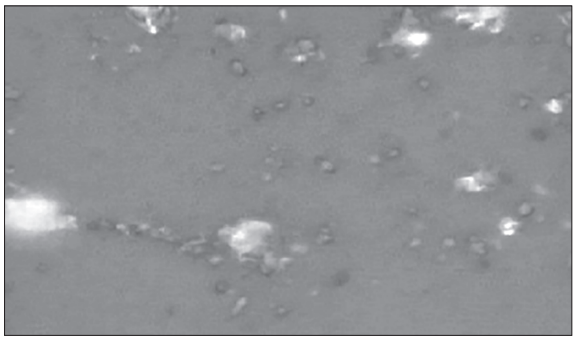

Fig. 23. The structure of the film surface synthesized on a glass substrate from the products of the sputtering of copper electrodes in air at atmospheric pressure for 30 minutes under the influence of nanosecond discharge factors (f = = 100 Hz) [14]

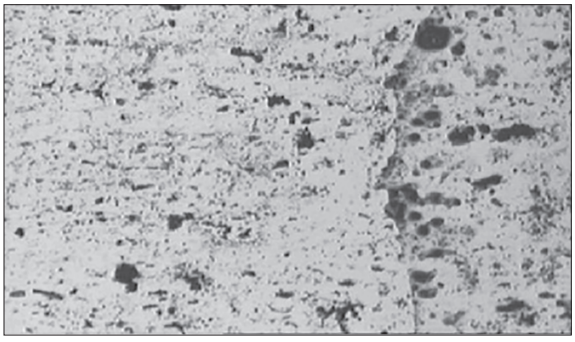

Fig. 24. The same as in the previous figure, but for zinc electrodes [69]

The study of the transmission (absorption) spectra of light by the deposited film nanostructures was carried out on an Ocean Optics USB-2000 spectrometer and was programmatically processed on a computer taking into account the absorption by a glass substrate.

The image of the surface of thin nanostructured films was recorded using a CrossBeam Workstation Auriga (Carl Zeiss) scanning electron microscope.

Raman spectra were excited with an argon ion laser, which generated radiation at a wavelength of 514.5 nm. Raman spectra of light scattering from thin-film nanostructures of transition metal oxides were recorded using nVia Renishaw spectrometer.

Figures 23 and 24 present images of the surfaces of films deposited from the plasma of an OND between metal electrodes in air or argon. To determine the size of the nanostructures, a gel based on standard spherical gold nanostructures with a diameter of 20 nm was applied to the film surface. Comparative analysis of the sizes of spherical gold nanostructures and nanostructures synthesized from nanosecond discharge products showed that the sizes of synthesized nanostructures are in the range of 2–20 nm. The cross-section of zinc-based nanostructures had dimensions predominantly in the range of 10–50 nm; the formation of micron-sized zinc agglomerates was also observed. The study of the cross-sectional surface of nanostructures and a glass substrate (in the

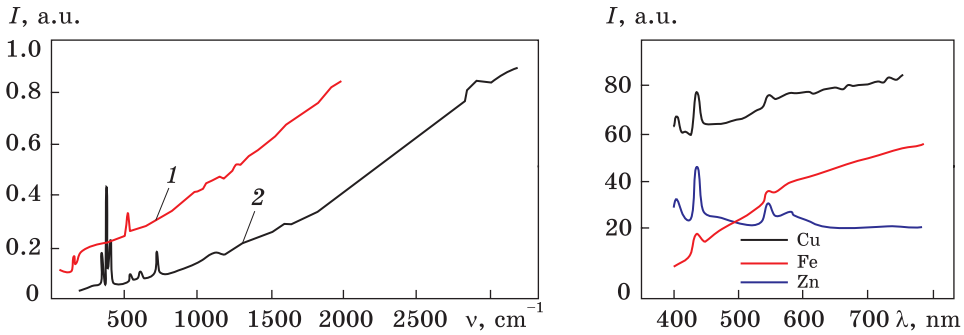

Fig. 25. Raman scattering spectra of zinc oxide nanostructures synthesized on a glass substrate based on sputtering products of zinc electrodes in air at atmospheric pressure for 30 minutes (*1*) and Raman scattering spectra of ZnO nanostructures on Al_2O_3 substrate (*2*) [14]

Fig. 26. Transmission spectra of films obtained by sputtering copper, iron, and zinc electrodes in air at atmospheric pressure [6, 14]

direction perpendicular to the substrate) has not been carried out, but, based on the known conditions for the synthesis of such nanostructures using a magnetron discharge, it is possible to assume that these can be nanowhiskers of copper or zinc oxides. At elevated air pressures and the energy contribution to the plasma (when using magnetrons, nanosecond discharges in liquid or air), the formation of nanodispersion or nanostructures of complex-shaped transition metal oxides is recorded [51–61, 68–71].

The cross section of nanostructures based on zinc oxide also had dimensions close to those of copper nanostructures, but the formation of micron-sized zinc agglomerates was also observed. The study of the cross-sectional surface of nanostructures and a glass substrate (in the direction perpendicular to the substrate) has not been carried out, but, based on the known conditions for the synthesis of such nanostructures using a magnetron discharge, it is possible to assume that these can be nanowhiskers of copper or zinc oxides.

Our hypothesis was confirmed for ZnO-based nanostructures after studying the Raman scattering spectrum of radiation from an argon ion laser at a wavelength of 514.5 nm and comparing it with the corresponding Raman scattering spectrum of the same laser radiation by nanopillars with ZnO. In paper [73], zinc oxide nanopillars were synthesized by the action of a high-power exciplex KrF laser with a generation wavelength of 248 nm on the surface of a ceramic target with ZnO, which was constantly rotating.

As follows from Fig. 25, the spectrum of Raman scattering of laser radiation from an Ar^+ laser that we obtained is in good agreement with the data of [72], where scattering by zinc oxide nanopillars with a diam-

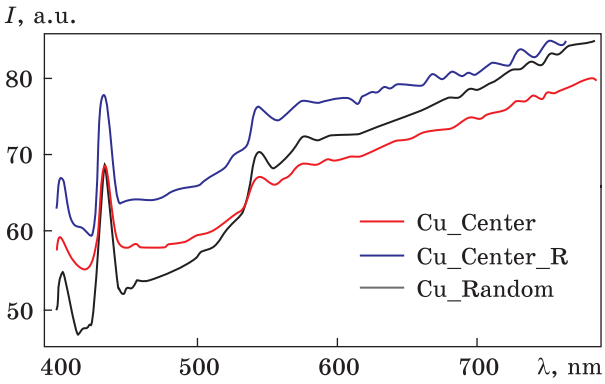

Fig. 27. Transmission spectrum of the film based on copper oxide nanostructures at localization of the spectrometer at various points of deposition [6, 14]

eter of 8–35 nm was studied. The differences in our Raman spectra and the data from Ref. [72] in the wavelength range 200–800 cm^{-1} are due to different types of substrates on which these nanostructures were synthesized. Therefore, with a high degree of probability, we can assume that, under our conditions, nanopillars with ZnO were synthesized directly onto a glass substrate without using transition film structures with nuclei for the growth of nanopillars.

The transmission spectrum of films based on nanostructures of zinc, copper and iron in the visible region of wavelengths is shown in Fig. 26 [74, 75]. The transmission of the films was studied in the middle of the radius of the substrate. It was found that films along the radius are rather inhomogeneous (Fig. 27), which is mainly due to gas-dynamic phenomena inside the discharge gap and the use of a point source of vapours of the electrode material. It is possible to improve the uniformity of deposited nanostructures with a substrate radius by moving the substrate relative to the discharge gap at a certain low speed and using a ruler from the discharge gaps when sputtering large-area films.

The general view of the transmission band of nanostructures, when the transmission of the film sharply increases in the visible region of the spectrum (continuum without maxima and minima from 500 to 700 nm) corresponds well to the transmission of cuprous oxide (Cu_2O) nanostructures [76]. The absorption band of the film in the wavelength range of 550–580 nm corresponds to the absorption band of copper nanostructures [77]. Narrow antireflection bands of the film in the blue part of the spectrum (at wavelengths of 420 and 450 nm) most likely are caused by the action of UV radiation of the discharge plasma in the spectral range of 200–230 nm. During the deposition of the film, the UV irradiation results in the radiation defects (see, *e.g.*, [78, 79]) in nanostructured films based on cuprous oxide and copper oxide and the formation of new energy levels of these compounds. Nanostructures of cuprous oxide and copper oxide as well as their colloidal solutions are

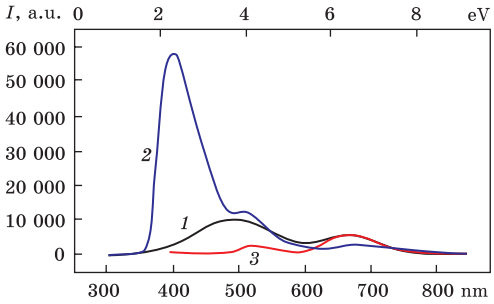

Fig. 28. Photoluminescence spectra of copper-based nanostructures upon their excitation by radiation with wavelengths of 270 (*1*), 330 (*2*), and 380 (*3*) nm [24, 72]

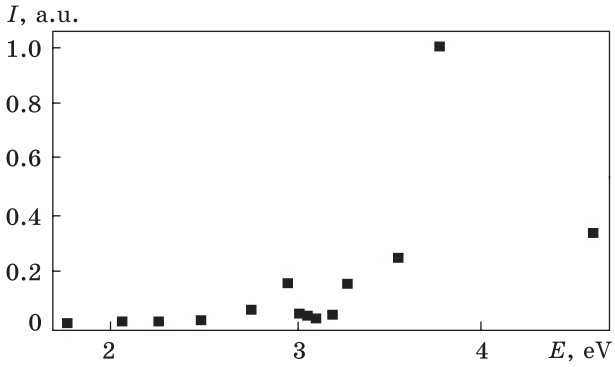

Fig. 29. The dependence of the photoluminescence radiation intensity on the exciting radiation energy [24, 72]

characterized by broad structureless transmission spectra in the ultraviolet, visible and near infrared wavelength regions [80, 81], but not narrow areas of bleaching that were observed in this experiment. The most intense antireflection bands were nanostructured films based on the products of sputtering of copper and zinc electrodes, which correlates with the selective and intense radiation of a nanosecond discharge in the spectral range of 200–230 nm. For a discharge between stainless steel electrodes, the selectivity and intensity of plasma radiation decrease, which also leads to a decrease in the antireflection peaks of films based on iron nanostructures (Fig. 26).

Figure 28 presents typical photoluminescence spectra of nanostructured films based on cuprous oxide and copper oxide. As Figure 28 demonstrates, there are three characteristic photoluminescence spectra for wavelengths when the luminescence intensity is significant.

The excitation wavelength is indicated on each band. The spectra shown start at the excitation wavelength and end at 850 nm. A characteristic feature of the lightening spectra is the presence of two broad emission bands of different intensities and different positions in the spectral range that was studied.

The photoluminescence spectra were characterized by two broad maxima in the spectral range of 400–600 nm, which shifted to the long-wavelength region of the spectrum and decreased in intensity when go-

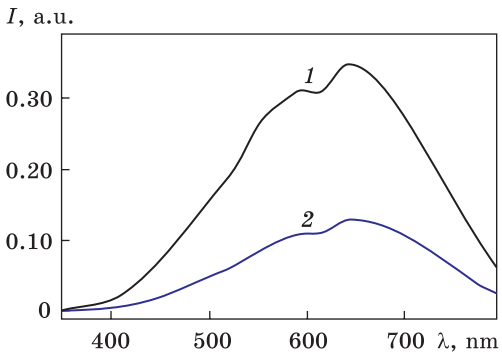

Fig. 30. Transmission spectra of the Cu- and Al-based films in the spectral region 350–800 nm (band lamp): *1* is glass substrate, *2* is film obtained by sputtering aluminium electrodes in a discharge on the nitrogen–oxygen mixture (p_{nitrogen}–p_{oxygen} = 100–1 kPa); the voltage pulse repetition rate is of 40 Hz, and the film deposition time is of 3 h [72, 81]

ing from the excitation wavelength at 330 nm, both to the region of 270 nm and to the region of 380 nm. It was pointed out in [12, 13] that assisting the growth of transparent conducting layers based on zinc oxide nanostructures by ultraviolet radiation from a mercury lamp improves their electrical characteristics by creating additional donor centres and reducing the scattering of charge carriers at grain boundaries of nanowhiskers. In our case, there is no need to use external sources of UV radiation, since the studied plasma itself is a selective emitter in the spectral range of 200–230 nm.

In order to carry out a certain quantitative analysis of the antireflection spectra, their brightness was calculated and analyzed as a function of the radiation energy with which the excitation was carried out. The brightness value is normalized for the range of the studied values. The calculation result is shown in Fig. 29. A qualitative analysis of the obtained dependence revealed a clear maximum at energy of 3.8 eV, which corresponds to a wavelength of 330 nm. This fact indicates the presence in the deposited objects in this energy range of a significant density of levels involved in radiative transitions in the 360–490 nm region, which is of considerable interest for research.

Figure 30 presents the transmission spectra of film samples on a glass plate of 1.4 mm thick in the range 350–800 nm (incandescent lamp), respectively. The spectra were obtained using the technique and measuring stand described in Ref. [82]. In glass plates, transmission spectra begin to be recorded at wavelengths λ exceeding 300 nm.

As follows from Fig. 30, the synthesized thin film is characterized by weak transmission of visible radiation. Studies of the characteristics of an OND showed that between the aluminium and chalcopyrite electrodes at argon pressures of 13.3 and 101 kPa, a diffuse discharge is ignited at the initial moments of time, which is further contracted, as evidenced by the presence of a characteristic spark continuum of radiation in the spectral region of 200–650 nm. The spark continuum of plasma radiation was most pronounced at an argon pressure of 101.3 kPa,

which indicates the contraction of the discharge after the first half-wave of the reflected voltage pulse because of the inconsistency of the plasma resistance with the resistance of the discharge power supply system. Therefore, for a more efficient use of the diffuse stage of the discharge, it is necessary to ignite it at pressures in the argon pressure range of 10–30 kPa.

The maximum pulsed electric power of the discharge reached 4 MW, and the energy contribution to the plasma in one pulse was 423 mJ. The study of the spectral characteristics of plasma based on the Ar–Al–$CuInSe_2$ vapour–gas mixtures showed that the most intense spectral lines of the copper atom in the range of 200–250 nm, and the spectral lines of atoms and ions of indium and aluminium were observed in the longer wavelength region of the spectrum. The nature of the plasma emission spectra does not allow one to assume the existence of such selective mechanisms of the formation of excited metal atoms and ions because of the transfer of energy from metastable atoms or argon molecules to atoms of aluminium, copper, or indium. To diagnose the deposition of films of quaternary chalcopyrite of the $CuIn_{1-x}Al_xSe_2$ type in real time, the following separately placed and most intense lines in the spectral range of 300–460 nm can be used: 307.38 Cu I, 329.05 Cu I, 410.17 In I, 451.13 nm In I, as well as 308.21, 309.27, 394.40, 396.15 nm Al I. The presence of the main spectral lines of aluminium, copper and indium in the plasma emission spectra allows one to assume the possibility of deposition of a thin film with the composition of the quaternary chalcopyrite $CuIn_{1-x}Al_xSe_2$ outside the plasma medium, as was realized for the ternary $CuInSe_2$ chalcopyrite.

According to Ref. [47], films based on nanostructured ceramics made of aluminium oxide are practically opaque in the visible region of the spectrum, their transmittance begins to increase only in the spectral range 0.8–2.0 μm from 1–3 to 25%. During the deposition of the destruction products of aluminium electrodes and oxygen molecules in air plasma on a glass substrate, thin films based on nanostructures of aluminium oxide were synthesized, which were characterized by low transparency in the visible region of the spectrum.

6. Summary and Conclusions

Thus, in the study of the characteristics of an overstressed bipolar nanosecond discharge of atmospheric pressure between electrodes made of transition metals the following is noteworthy.

- An intense nanosecond discharge in air between zinc and copper electrodes is a selective source of UV radiation in the spectral ranges of 200–215 nm and 200–230 nm, respectively. Discharge radiation between stainless steel electrodes filled a relatively wide spectral range of

200–300 nm. The maximum pulsed energy contribution to the plasma was reached as 4 MW, and the energy introduced into the discharge in one pulse reached 0.1 J. The most probable mechanism for the excitation of UV radiation of atoms and ions of transition metals is the ectonic mechanism of erosion of the metal electrodes' surface, the excitation and ionization of atoms and ions of transition metals by electron impact, as well as the formation of excited atoms and metal ions in the processes of electron–ion recombination of singly and doubly charged metal ions with electrons.

- The plasma of an OND between aluminium electrodes at air pressures of 50–202 kPa, a pulsed discharge power of 3–6.5 MW, and an energy contribution of 110–153 mJ per discharge pulse is a source of electroluminescence of aluminium oxide nanoparticles in the form of a wide band, which is located in the spectral range of 300–430 nm. During the deposition of the products of destruction of electrodes and air molecules in plasma on a glass substrate, thin films based on aluminium oxides (Al_2O_3) are synthesized, which are characterized by low transparency in the visible wavelength range.
- At an argon pressure of 100 kPa between copper electrodes and an interelectrode distance of 2 mm, a sufficiently homogeneous overstressed nanosecond discharge with a pulsed electric power of up to 1.2 MW was ignited, and the energy contribution to the plasma in one pulse was of 176 mJ. Studies of the spectral characteristics of plasma based on the copper–argon vapour–gas mixtures showed that the most intense were the spectral resonance spectral lines of the copper atom (λ = 324.75 and 327.39 nm Cu I) from the lines of a singly charged copper ion in the range of 200–330 nm, and the most intense was the spectral line λ = 227.62 nm Cu II; automatic irradiations of the substrate and film nuclei on the substrate with hard UV radiation of copper atoms and ions from the discharge plasma are promising for influencing the electrical characteristics of the synthesized films, in particular, reducing their resistance.
- As found, at an argon pressure of 200 kPa between a copper electrode and a zinc electrode at an interelectrode distance of 2 mm, an overstressed nanosecond discharge uniform in space with a pulsed electric power of up to 2.5 MW was ignited with an energy contribution to the plasma in one pulse of ≈374 mJ.
- The study of the spectral characteristics of plasma based on the copper–zinc–argon vapour–gas mixtures showed that the most intense were the spectral resonance spectral lines of the copper atom (λ = 324.75 and 327.39 nm Cu I) from the lines of a singly charged copper ion in the range 200–330 nm, the most intense there was a line λ = 227.62 nm Cu II. The line with λ = 618.86 nm Cu II was distinguished from ionic spectral lines in the visible spectral region. The introduction of zinc

vapour into the discharge made it possible to offset the short-wavelength boundary of the emission spectrum to 202–207 nm due to the intense ionic lines of zinc and to enrich the spectrum of UV radiation of plasma with intense spectral lines 258.24, 268.41, 271.24, and 275.64 nm Zn I. An increase in the Ar pressure from 50 to 200 kPa leads to increasing the intensity of most of the spectral lines of Cu and Zn. The presence in the emission spectrum of plasma based on vapour–gas mixtures 'copper–zinc–argon' creates the necessary conditions for the deposition of composite films of the Cu–Zn type on a substrate installed near the electrode system.

- Studying the characteristics of an OND showed that between the aluminium and chalcopyrite electrodes at an argon pressure of 100 kPa, a diffuse discharge is ignited at the initial moments of time, which is further contracted, as evidenced by the presence of a characteristic spark continuum of radiation in the spectral region of 200–650 nm. The spark continuum of plasma radiation was most pronounced at an argon pressure of 100 kPa, which indicates the contraction of the discharge after the first half-wave of the reflected voltage pulse because of the mismatch of the plasma resistance with the resistance of the discharge power supply system. The maximum pulsed electrical power of the discharge reached 4 MW, and the energy contribution to the plasma in one pulse was 423 mJ. Studies of the spectral characteristics of plasma based on the Ar–Al–$CuInSe_2$ vapour–gas mixtures showed that the most intense spectral lines of the copper atom in the range of 200–250 nm, and the spectral lines of atoms and ions of indium and aluminium were observed in the longer wavelength region of the spectrum. To diagnose the deposition of films of quaternary chalcopyrite of the $CuIn_{1-x}Al_xSe_2$ type in real time, the following separately placed and most intense lines in the spectral range of 300–460 nm can be used: 307.38 Cu I, 329.05 Cu I, 410.17 In I, 451.13 nm In I, and also 308.21, 309.27, 394.40, 396.15 nm Al I. The presence in the plasma emission the spectra of the main spectral lines of Al, Cu, and In allows one to assume the possibility of deposition of a thin film with the composition of the quaternary chalcopyrite $CuIn_{1-x}Al_xSe_2$ outside the plasma medium.

As found for an OND between copper electrodes in argon at atmospheric pressure, the maximum value of the average power of UV radiation was observed for the UV-A range, and the absolute radiation densities in various UV ranges reached as follow: in UV-C, 67 mW/m^2, in UV-B, 65 mW/m^2, and in UV-A, 204 mW/m^2. For a discharge at p_{Ar} = 6.7 kPa, the radiation power decreased by more than an order of magnitude. The most effective was an increase in the pulse repetition rate up to 1000 Hz, rather than an increase in the value of the charging voltage on the working capacitor of the high-voltage modulator, but, when the UV-radiation source operates in the frequency range

of 300–1000 Hz, it is necessary to use forced cooling of the discharge device.

Based on the results of an experimental study of the spectral characteristics of air plasma in an OND between Cu electrodes, at air pressures in the range of 30–200 kPa, it is shown that the calculated values of the temperature and concentration of electrons are 2.4–3.7 eV (T_e) and 10^{15}–10^{18} cm^{-3} (n_e). With an increase in the air pressure in the discharge gap of 1 mm from 30 to 200 kPa, the concentration of doubly charged atomic nitrogen ions decreased from 10^{16} to 10^{13} cm^{-3}. The results obtained also make it possible to judge the energy aspects of electrode sputtering, typical concentrations of the atomic and ionic components of plasma, and the possible effect of chemical processes in the technological application of this type of discharge in air.

Thin films based on nanostructures of copper, zinc and oxides of copper, zinc with dimensions of 2–40 nm are synthesized. As found, when assisting the deposition of copper films by UV radiation of plasma in the spectral range of 200–230 nm, narrow bands of antireflection of the films are formed at wavelengths of 420 and 450 nm. This may be due to the formation of radiation defects in these films. It was revealed photoluminescence of nanostructured copper films in the visible spectral range, which was characterized by two maxima at wavelengths in the spectral range of 400 and 520 nm, when it was excited by photons with an energy of 3.8 eV (at a wavelength of 330 nm), for photons with an energy of 2.95 eV. A secondary maximum of lower amplitude was observed in the luminescence efficiency of the films under the action of a high-pressure mercury-arc lamp.

REFERENCES

1. J.P. Walters and H.V. Malmstadt, *Analytical Chemistry*, **37**, No. 12: 1484 (1965); https://doi.org/10.1021/ac60231a010
2. L.F. Strelkov and A.A. Yankovski, *Journal of Applied Spectroscopy*, **19**, No. 4: 605 (1973); https://doi.org/10.1007/BF00604063
3. L.P. Babich, T.V. Loiko, and V.A. Zuckerman, *Physics-Uspekhi*, **160**, No. 7: 49 (1990); https://doi.org/10.3367/UFNr.0160.199007b.0049.
4. V.V. Akhmadeev, L.M. Vasilyak, S.V. Kostyuchenko, N.N. Kudryavtsev, and G.A. Kurkin, *Journal of Technical Physics*, **66**, No. 4: 58 (1996).
5. A.K. Shuaibov, G.E. Laslov, and Ya.Ya. Kozak, *Optics and Spectroscopy* **116**, No. 4: 552 (2014); https://doi.org/10.1134/S0030400X14030199
6. A.K. Shuaibov, A.Y. Minya, A.A. Malinina, A.N. Malinin, V.V. Danilo, M.Yu. Sichka, and I.V. Shevera, *American Journal of Mechanical and Materials Engineering*, **2**, 1: 8 (2018); https://doi.org/10.11648/j.ajmme.20180201.12

7. A.K. Shuaibov, A.I. Minya, Z.T. Gomoki, and V.V. Danilo, and P.V. Pinzenik, *Surface Engineering and Applied Electrochemistry*, **55**, No. 1: 65 (2019); https://doi.org/10.3103/S1068375519010137
8. G.A. Mesyats, *Physics-Uspekhi*, **38**, 6: 567 (1995); https://doi.org/10.1070/PU1995v038n06ABEH000089
9. A.R. Striganov and N. Sventitsky, *Tables of Spectral Lines of Neutral and Ionized Atoms* (Moscow: Atomizdat: 1966) (in Russian).
10. *NIST Atomic Spectra Database Lines Form*; https://physics.nist.gov/PhysRefData/ASD/lines_form.html
11. O.K. Shuaibov, O.I. Minya, Z.T. Gomoki, and V.V. Daniil, *Method for Nanostructuring a Glass Surface in Atmospheric Pressure Air*: Patent UA 05112 (Publ. Bull. No. 21, 2017) (in Ukrainian).
12. O.H. Abduev, A. Sh. Asvarov, N.M. Alikhanov, V.V. Belyaev, and F.I. Vysikaylo, *Physical Electronics: Proc. IX All-Russian Conf.* (2016, Makhachkala) (ITC DTU: 2016), p. 265.
13. A.Kh. Abduev, A.Sh. Asvarov, A.K. Akhmedov, R.M. Emirov, and V.V. Belyaev, *Technical Physics Letters*, **43**, No. 22: 40 (2017); https://doi.org/10.21883/PJTF.2017.22.45259.16874
14. A. Shuaibov, A. Minya, A. Malinina, A. Malinin, R. Golomd, I. Shevera, Z. Gomoki, and V. Danilo, *Advances in Natural Sciences: Nanoscience and Nanotechnology*, **9**: 035018 (2018); https://doi.org/10.1088/2043-6254/aadc4b
15. E.M. Egorova, *Biological Effects of Metal Nanoparticles* (Moscow: Nauka: 2014) (in Russian).
16. V.F. Tarasenko, E.Kh. Baksht, A.G. Burachenko, and M.I. Lomaev, *Plasma Physics Reports*, **43**: 792 (2017); https://doi.org/10.1134/S1063780X17070121
17. D.Z. Pai, D.A. Lacoste, and Ch.O. Laux, *Plasma Sources Science and Technology*, **19**: 065015 (2010); https://doi.org/10.1088/0963-0252/19/6/065015
18. K.A. Prilepa, A.V. Samusenko, and Yu.K. Stishkov, *High Temperature*, **54**: 655 (2016); https://doi.org/10.1134/S0018151X16040192
19. O.K. Shuaibov, V.V. Danilo, O.Y. Minya, A.O. Malinina, and S.Yu. Naymet, *Scientific Herald of Uzhhorod University. Series 'Physics'*, No. 44: 154 (2018) (in Ukrainian); https://doi.org/10.24144/2415-8038.2018.44.154-164
20. O.K Shuaibov, O.Y. Minja, M.P.Chuchman, Z.T. Homoki, and V.V. Danylo, *NSC 'Kharkiv Institute of Physics and Technology' and Bogolyubov Institute for Theoretical Physics Scientific Council 'Plasma Physics and Plasma Electronics' 2017 Annual Report* (Kyiv: 2018), p. 54 (in Ukrainian).
21. A.K. Shuaibov, A.Y. Minya, Z.T. Gomoki, V.V. Danilo, and R.B. Pynzenik, *Electronic Material Processing*, **54**, No. 1: 46 (2018) (in Russian); https://doi.org/10.5281/zenodo.1168351
22. O.K. Shuaibov, O.Y. Minya, Z.T. Gomoki, V.V. Danilo, *Windowless, Spot, Ultraviolet Lamp on Copper Vapors*: Patent UA 10.04.2018 (Publ. Bull. No. 7, 2018) (in Ukrainian).
23. O.Y. Minya, O.K. Shuaibov, Z.T. Gomoki, V.V. Danilo, M.M. Chavarga, and L.E. Kukri, *Scientific Herald of Uzhhorod University. Series 'Physics'*, No. 39: 93 (2016) (in Ukrainian); https://doi.org/10.24144/2415-8038.2016.39.93-99

24. A.K. Shuaibov, A.Y. Minya, A.A. Malinin, A.N. Malinin, Z.T. Gomoki, I.V. Shevera, and V.V. Danilo, *Electronic Processing of Materials*, **55**, No. 4: 56 (2019) (in Russian);
https://doi.org/10.5281/zenodo.3369706
25. O. Shuaibov, V. Chyhin, A. Malinina, V. Danylo, and V. Chynin, *Herald of Khmelnytskyi National University. Technical Sciences*, **4**, 209 (2019);
http://journals.khnu.km.ua/vestnik/wp-content/uploads/2021/01/35-7.pdf
26. V.V. Danilo, O.K. Shuaibov, O.Y. Minya, Z.T. Gomoki, I.V. Shevera, A.O. Malinina, and O.M. Malinin, *Int. Conf. Scientists and Post-Graduates Institute of Electron Physics–IEP-2019 (21–24 May, 2019, Uzhhorod)*, p. 61.
27. A.A. Malinina, A.K. Shuaibov, A.Y. Minya, A.N. Malinin, R.V. Hritsak, I.V. Shevera, and V.V. Danilo, *Int. Conf. Scientists and Post-Graduates Institute of Electron Physics–IEP-2019 (21–24 May, 2019, Uzhgorod)*, p. 87.
28. V.F. Tarasenko, *Runaway Electrons Preionized Diffuse Discharge* (New York: Nova Science Publishers Inc.: 2014).
29. A. Omarov, V.S. Kurbanismailov, G.B. Ragimkhanov, M.Kh. Gadzhiev, and M.V. Kurbanismailov, *Bulletin of the Dagestan University*, **6**: 5 (2012) (in Russian).
30. V.S. Kurbanismailov, O.A. Omarov, and G.B. Ragimkhanov, *Prikladnaya Fizika*, **2**: 35 (2014) (in Russian).
31. O.A. Omarov, N.O. Omarova, P.Kh. Omarova, and A.A. Aliverdiev, *High Temperature*, **57**: 156 (2019);
https://doi.org/10.1134/S0018151X19020159
32. O.K. Shuaibov, A.A. Malinina, and A.N. Malinin, *Characteristics and Parameters of Overvoltage of a Nanosecond Discharge in Vapor–Gas Sums and the Development of New Gas-Discharge Lamps* (Uzhgorod: Uzhhorod National University–Publishing House 'Hoverla': 2021) (in Ukrainian).
33. O.Y. Minya. V.M. Krasilinets, O.K. Shuaibov, I.V. Shever, Z.T. Gomoki, M.M. Chavarga, A.M. Solomon, and V.I. Mikla, *Scientific Herald of Uzhhorod University. Series 'Physics'*, No. 46: 84 (2019);
https://doi.org/10.24144/2415-8038.2019.46.84-91
34. O.K. Shuaibov, O.Y. Minya, M.P. Chuchman, A.O. Malinina, O.M. Malinin, V.V. Danilo, and Z.T. Gomoki, *Ukrainian Journal of Physics*, **63**, No. 9: 790 (2018);
https://doi.org/10.15407/ujpe63.9.790
35. O.K. Shuaibov, A.O. Malinina, and O.M. Malinin, *New Gas-Discharging Methods of Obtaining Selective Ultraviolet and Visible Radiation and Synthesis of Nanostructures of Oxides of Transition Metals* (Uzhgorod: Uzhhorod National University–Publishing House 'Hoverla': 2019) (in Ukrainian).
36. D.V. Beloplotov, M.I. Lomaev, D.A. Sorokin, and V.F. Tarasenko, *Journal of Technical Physics*, **88**, No. 6: 819 (2018) (in Russian);
https://doi.org/10.21883/JTF.2018.06.46032.2465
37. D.V. Beloplotov, V.I. Lomaev, D.A. Sorokin, and V.F. Tarasenko, *Journal of Physics: Conference Series*, **652**: 012012 (2015);
https://doi.org/10.1088/1742-6596/652/1/012012
38. D.V. Beloplotov, M.I. Lomaev, and V.F. Tarasenko, *Atmospheric and Oceanic Optics*, **28**: 476 (2015);
https://doi.org/10.1134/S1024856015050024
39. D.V. Beloplotov, V.F. Tarasenko, and M.I. Lomaev, *Atmospheric and Oceanic Optics*, **29**, No. 2: 96 (2016) (in Russian);
https://doi.org/10.15372/AOO20160202

40. S.I. Maximov, A.V. Kretinina, N.S. Fomina, and L.N. Gall, *Scientific Instrument Making*, **25**, No. 1: 36 (2015).
41. V.I. Tyutyunnikov, *East European Journal of Physics*, **2**, No. 3: 64 (2015); https://periodicals.karazin.ua/eejp/article/view/4450
42. A.M. Ampilov, E.M. Barkhudarov, Yu.N. Kozlov, I.A. Kossy, and M.A. Misyakan, *Plasma Physics Reports*, **45**, No. 3: 246 (2019); https://doi.org/10.1134/S036729211902001X
43. A.K. Shuaibov, A.I. Minya, A.A. Malinina, and A.N. Malinin, *Abstracts of the 6th Int. Sci. Practical Conf. 'Science, Society, Education: Topical Issues and Development Prospects'* (Kharkiv: 2020), p. 323.
44. A. Shuaibov, A. Minya, A. Malinina, A. Malinin, and Z. Gomoki, *Highlights in BioScience*, **3**: 20211 (2020); https://doi.org/10.36462/H.BioSci.20211
45. A.E. Egorov and V.V. Chernyshev, *Bulletin of the Voronezh State University. Series Physics and Mathematics*, **2**: 8 (2005).
46. V.S. Kortov, A.E. Ermakov, A.F. Zatsepin, M.A. White, and S.V. Nikiforov, *Solid State Physics*, **50**, No. 5: 916 (2008).
47. I.V. Gassenkova, N.I. Mukhurov, and Ya.M. Vahioh, *Doklady BGUIR*, No. 2: 114 (2016) (in Russian); https://doklady.bsuir.by/jour/article/view/639/639
48. A.N. Gomonai, *Journal of Applied Spectroscopy*, **82**: 13 (2015); https://doi.org/10.1007/s10812-015-0057-4
49. D. Levko and L.L. Raja, *Physics of Plasmas*, **22**, No. 12: 123518 (2016); https://doi.org/10.1063/1.4939022
50. J. Lypez-Garcна, M. Placidi, X. Fontanй, V. Izquierdo-Roca, M. Espindola, E. Saucedo, C. Guillйn, J. Herrero, and A. Pйrez-Rodriguez, *Solar Energy Materials and Solar Cells*, **132**: 245 (2015); https://doi.org/10.1016/j.solmat.2014.09.003
51. R.V. Hrytsak, A.O. Malinina, O.J. Minya, O.K. Shuaibov, and S.Y. Neymet, *XIX International Young Scientists Conference on Applied Physics (21–25 May, 2019, Kyiv)* (Kyiv: Taras Shevchenko National University of Kyiv: 2019), p. 71.
52. 52.A.K. Shuaibov, A.Y. Minya, Z.T. Gomoki, R.V. Hrytsak, A.A. Malinina, and A.N. Malinin, *Journal of Physics and Chemistry Research*, **1**, No. 9: 1 (2019).
53. A.K. Shuaibov, A.I. Minya, A.A. Malinina, R.V. Gritsak, and A.N. Malinin, *Ukrainian Journal of Physics*, **65**, No. 5: 400 (2020); https://doi.org/10.15407/ujpe65.5.400
54. A.K. Shuaibov, A.Y. Minya, R.V. Hrytsak, A.A. Malinina, and A.N. Malinin, *Advances in Nanoscience and Nanotechnology*, **4**, No. 1: 1 (2020).
55. A.K. Shuaibov, A.Y. Minya, Z.T. Gomoki, A.A. Malinina, A.N. Malinin, V.V. Danilo, Yu.Yu. Bilak, and Ya.Ch. Kolozhvari, *HSOA Journal of Biotech Research & Biochemistry*, **3**, No. 1: 100005 (2020).
56. A.K. Shuaibov, A.Y. Minya, Z.T. Gomoki, R.V. Hrytsak, A.A. Malinina, A.N. Malinin, V.M. Krasilinets, and V.M. Solomon, *Surface Engineering and Applied Electrochemistry*, **56**: 474 (2020); https://doi.org/10.3103/S1068375520040158
57. A.K. Shuaibov, A.Y. Minya, M.P. Chuchman, A.A. Malinina, A.N. Malinin, T.Z. Gomoki, and Y.Ch. Kolozvari, *Plasma Research Express*, **1**: 015003 (2018); https://doi.org/10.1088/2516-1067/aae5ca
58. A.O. Malinina, R.V. Grytsak, O.K. Shuaibov, O.Y. Mynya, and O.M. Malinin, *8th Int. Conf. 'Medical Physics – Successful Development, Problems, New Technologies' (26–27 September, 2019, Kyiv, Ukraine)*, p. 216 (in Ukrainian).

59. O.K. Shuaibov, O.Y. Minya, Z.T. Gomoki, R.V. Hrytsak, A.O. Malinina, and O.M. Malinin, *Methods for the Synthesis of Thin Chalcopyrite Films in an Acid-Free Gas Medium*: Patent UA 142634 (Publ. 25.06.2020, Bull. No. 12, 2018) (in Ukrainian).
60. I.E. Kacher, A.K. Shuaibov, M.Yu. Rigan, and A.I. Dashchenko, *High Temperature*, **40**: 814 (2002); https://doi.org/10.1023/A:1021412930269
61. R. Shuker, Y. Binur, and A. Szцke, *Phys. Rev. A*, **12**, No. 2: 512 (1975); https://doi.org/10.1103/PhysRevA.12.515
62. L.M. Biberman, V.S. Vorobiev, and I.T. Yakubov, *Kinetics of Nonequilibrium Low-Temperature Plasma* (Moscow: Nauka: 1982) (in Russian).
63. W. Lochte-Holtgreven, *Plasma Diagnostics* (Amsterdam: North-Holland: 1968).
64. M. Chuchuman, L. Mesarosh, and A. Shuaibov, *Optics*, **4**, No. 5: 31 (2015); https://doi.org/10.11648/j.optics.20150405.11
65. P. Szroeder, I. Sahalianov, T. Radchenko, V. Tatarenko, and Yu. Prylutskyy, *Optical Materials*, **96**: 109284 (2019); https://doi.org/10.1016/j.optmat.2019.109284
66. I.Yu. Sahalianov, T.M. Radchenko, V.A. Tatarenko, Yu.I. Prylutskyy, *Annals of Physics*, **398**: 80 (2018); https://doi.org/10.1016/j.aop.2018.09.004
67. T.M. Radchenko, V.A. Tatarenko, and G.Cuniberti, *Materials Today: Proceedings*, **35**, Pt. 4: 523 (2021); https://doi.org/10.1016/j.matpr.2019.10.014
68. A.K. Shuaibov, M.P. Chuchmana, and L.V. Mesarosh, *Surface Engineering and Applied Electrochemistry*, **54**, No. 3: 267 (2018); https://doi.org/10.3103/S1068375518030122
69. A. Shuaibov, A. Minya, A. Malinina, Z. Gomoki, and V. Danilo, *Journal of Physics and Chemistry Research*, **1**, No. 1: 1 (2019).
70. A. Shuaibov, A. Minya, I. Shevera, A. Malinina, R. Gritsak, A. Malinin, Z. Gomoki, and V. Danilo, *Highlihts in BioScience*, **3**: 1 (2020); https://doi.org/10.36462/H.BioSci.20207
71. N.A. Bulychev, M.A. Kazaryan, L.L. Chaikov, I.S. Burkhanov, and V.I. Krasovskii, *Bulletin of the Lebedev Physics Institute*, **41**: 264 (2014); https://doi.org/10.3103/S106833561409005X
72. A.K. Shuaibov, Y. Minya, Z.T. Gomoki, A.A. Malinina, A.N. Malinin, I.V. Shevera, and V.V. Danilo, *Surface Engineering and Applied Electrochemistry*, **56**: 210 (2020); https://doi.org/10.3103/S106837552004016X
73. V.E. Kaydashev, E.M. Kaydashev, M. Peres, T. Monteiro, M.R. Correia, and N.A. Sobolev, *Journal of Technical Physics*, **79**, No. 11: 45 (2009).
74. I.V. Shevera, O.I. Nalima, A.K. Shuaibov, M.Yu. Sechka, V.V. Danilo, and Z.T. Gomoku, *Proc. Int. Conf. of Young Scientists and Graduate Students (May 23–26, 2017, Uzhgorod)*, p. 152.
75. O. Mynia, A. Shuaibov, R. Holomb, V. Danylo, I. Shevera, and V. Mitsa, *Proc. XIII Int. Conf. 'Electronics and Applied Physics' (October 24–27, 2017, Kyiv, Ukraine)* (Kyiv: Taras Shevchenko National University of Kyiv: 2017), p. 153.
76. E.N. Zamanova and L.A. Aliyeva, *Fizika*, **XIV**, No. 3: 194 (2008).
77. B. Farmanfarmaei, M.R. RashidianVaziri, and F. Hajiesmaeilbaigi, *Quantum Electronics*, **44**, 11: 1029 (2014); https://doi.org/10.1070/QE2014v044n11ABEH015308

78. T.M. Radchenko, V.A. Tatarenko, V.V. Lizunov, V.B. Molodkin, I.E. Golentus, I.Yu. Sahalianov, and Yu.I. Prylutskyy, *Physica Status Solidi B*, **256**, No. 5: 1800406 (2019);
https://doi.org/10.1002/pssb.201800406
79. I.Yu. Sahalianov, T.M. Radchenko, V.A. Tatarenko, and G. Cuniberti, *EPL*, **132**, No. 4: 48002 (2020);
https://doi.org/10.1209/0295-5075/132/48002
80. D.A. Kudryashov, A.S. Gudovskikh, A.V. Babichev, A.V. Filimonov, A.M. Mozharov, V.F. Agekyan, E.V. Borisov, A.Yu. Serov, and N.G. Filosofov, *Physics and Technology of Semiconductors*, **51**: 110 (2017);
https://doi.org/10.1134/S1063782617010110
81. A.K. Shuaibov, A.Y. Minya, A.A. Malinina, A.N. Malinin, Z.T. Gomoki, V.V. Danylo, and Yu.Yu. Bilak, *Journal of Metallic Material Research*, 3, No. 2: 37 (2020);
https://ojs.bilpublishing.com/index.php/jmmr/article/view/2441
82. V.M. Holovey, K.P. Popovych, M.V. Prymak, M.M. Birov, V.M. Krasilinets, and V.I. Sidey, *Physica B*, **450**: 32 (2014);
https://doi.org/10.1016/j.physb.2014.05.059

Received 14.02.2021;
in final version, 01.07.2021

О.К. Шуаібов, А.О. Малініна
ДВНЗ «Ужгородський національний університет»,
Народна площа, 3, 88000 Ужгород, Україна

ПЕРЕНАПРУЖЕНИЙ НАНОСЕКУНДНИЙ РОЗРЯД У ГАЗАХ ЗА АТМОСФЕРНОГО ТИСКУ ТА ЙОГО ЗАСТОСУВАННЯ ДЛЯ СИНТЕЗУ НАНОСТРУКТУР НА ОСНОВІ ПЕРЕХІДНИХ МЕТАЛІВ

В оглядовій статті наведено характеристики та параметри перенапруженого наносекундного розряду між електродами з цинку, міді й алюмінію у повітрі й аргоні за атмосферного тиску. Представлено методику, техніку й умови експериментів з дослідження характеристик і параметрів перенапруженого наносекундного розряду та його застосування для синтезу тонких наноструктурованих плівок оксидів перехідних металів, синтезованих в умовах інтенсивного ультрафіолетового (УФ) опромінення підкладинки з плівкою. Джерелом парів металів у плазмі стають мікровибухи неоднорідностей на поверхні електродів у сильному електричному полі. Наведено просторові, електричні й оптичні характеристики перенапруженого наносекундного розряду у повітрі й аргоні між електродами з перехідних металів, який запалювався в системах електродів «голка–голка». Наведено результати експериментального міряння параметрів плазми розряду на основі газопарових сумішей Cu–повітря. Розглянуто оптичні характеристики тонких наноструктурованих плівок оксидів перехідних металів, синтезованих в умовах автоматичного УФ-опромінення підкладинки плазмою розряду.

Ключові слова: перенапружений наносекундний розряд, цинкові, мідні й алюмінійові електроди, тонкі наноструктуровані плівки.